Multiomics reveals an essential role of long-distance cadmium translocation in regulating plant cadmium resistance and grain cadmium accumulation in allohexaploid wheat (Triticum aestivum L.) genotypes

Ying-peng Hua
Zhengzhou University
Jun-fan Chen
Zhengzhou University
Dan-dan Shen
Zhengzhou University
Ting Zhou
Zhengzhou University
Ying-na Feng
Zhengzhou University
Shao-min Huang
Henan Academy of Agricultural Sciences
Zheng-fu Zhou
Henan Academy of Agricultural Sciences
Caipeng Yue (yuecaipeng@zzu.edu.cn)
Zhengzhou University https://orcid.org/0000-0001-9234-262X
Jin-yong Huang
Zhengzhou University

Research Article

Keywords: Allohexaploid wheat, genotypic differences, long-distance translocation, multiomics, Cd resistance and accumulation

Posted Date: February 23rd, 2022

DOI: https://doi.org/10.21203/rs.3.rs-1352596/v1

Abstract

Cadmium (Cd) easily enters cereal roots and is translocated to the shoots and grains thus posing risks to human health. Vastness and complexity of the allothexaploid wheat genome is a huge challenge for understanding its Cd resistance and accumulation. Herein, wheat plants of a Cd-resistant genotype ('ZM1860') and a Cd-sensitive genotype ('ZM32'), selected from 442 wheat cultivars, exhibited significantly differential plant Cd resistance. Integrated comparative analyses of morpho-physiological investigation, ionomic and phytohormone profiling, genomic variations, transcriptomic landscapes, and functional analysis was performed to identify the mechanisms underlying differential Cd resistance. Under Cd toxicity, 'ZM1860' outperformed than 'ZM32' with obvious leaf chlorosis, weaker root architecture, ROS over-accumulation, and disordered phytohormone homeostasis. Ionomics showed that 'ZM32' had a higher translocation coefficient of Cd from roots to shoots and accumulated more Cd in grains than 'ZM1860'. Whole-genome re-sequencing (WGS) and transcriptome sequencing identified numerous DNA variants and differentially expressed genes involved in abiotic stress responses and ion transport. Integrated ionomics, transcriptomics, and functional analyses identified the plasma membrane-localized TaHMA2b-7A as a central Cd exporter regulating differential long-distance Cd translocation in wheat genotypes. WGS- and PCR-based sequence polymorphisms revealed a 25-bp InDel site in the promoter region that might determine the differential gene expression of *TaHMA2b-7A* with same amino acid sequences in wheat gonotypes. The multi-omics approach used here eased the identification of wheat core transporters involving long-distance Cd translocation, and may provide elite gene resources for the genetic improvement of plant Cd resistance and grain Cd accumulation in wheat and other cereal species.

Key Message

A multiomics approach eased the identification of core transporters involving long-distance Cd translocation in allohexaploid wheat, which will provide elite gene resources for genetic improvement of wheat Cd resistance and grain Cd accumulation.

Introduction

Cadmium (Cd), a nonessential and typical toxic heavy metal, is one of the most dangerous and widespread contaminants in the environment **(Xu et al. 2022)**. It is commonly released into the soil through anthropogenic activities such as fertilization, urban and industrial discharges, and natural resources such as mines and volcanoes **(El Rasafi et al. 2020)**.

Cd is highly transferable in soils, thereby enabling it to be easily taken up by roots and rapidly transported to various plant tissues. Excessive Cd accumulation in plants can not only hamper plant growth and productivity but also eventually threaten animal and human health through the food chain **(Zhang et al. 2020)**. Understanding the mechanisms controlling Cd distribution in planta is essential to develop phytoremediation approaches as well as for food safety.

Bread wheat (*Triticum aestivum* L.) is one of the world's most important staple cereals for more than half of the world's population **(Qin et al. 2021)**. Cd is highly toxic to wheat plants, which show obvious reduction in seed germination and shoot/root growth **(Rizwan et al. 2016)**. Compared with rice, bread wheat appears to have a lower rate of Cd uptake by roots but a higher rate of Cd translocation from roots to shoots **(Sui et al. 2018)**. Screening wheat cultivars, with stably strong plant Cd resistance and low Cd accumulation in grains, is one of the most feasible and effective approaches to ensure food safety and quality. A number of studies have investigated the physiological aspects of plant Cd resistance and grain Cd accumulation in wheat **(Abedi and Mojiri 2020)**. However, the molecular mechanisms underpinning these processes remain largely elusive with hindered by the hexaploid nature, and the large size (about 17 Gb) and complexity (> 85% repetitive DNA) of the wheat genome (AABBDD, 2n = 6x = 42) **(International Wheat Genome Sequencing Consortium 2018).**

Accumulation and detoxification of Cd is regulated by several transport processes, including apoplastic influx into root tissues, root symplastic uptake, vacuolar sequestration, xylem loading, and cell wall adsorption, among others **(Raza et al. 2020)**. Cd^{2+} is mainly absorbed by plasma membrane-localized transporter NRAMP5 (Natural Resistance Associated Macrophage Protein 5) **(Sasaki et al. 2012)**.

The type 1_B subfamily of the P-type ATPases, namely $P1_B$-ATPase, is involved in heavy metal transport across cellular membranes **(Hussain et al. 2004)**. Arabidopsis has eight genes encoding P_{1B}-ATPases (heavy metal ATPases [HMA]), which are named as HMA1 to HMA8 proposed by **Baxter et al. (2003)**. $P1_B$-ATPases transport mono- (Cu^+/Ag^+) and divalent ($Cd^{2+}/Pb^{2+}/Zn^{2+}/Co^{2+}$) cations **(Cobbett et al. 2003)**. HMA2 and HMA4, function redundantly to translocate Cd from the roots to aerial tissues, probably by export into the xylem **(Colangelo et al. 2006)**. HMA3 is a tonoplast-localized transporter for Cd^{2+} in the roots and limited Cd^{2+} in roots **(Sasaki et al. 2014)**. Overexpression of rice OsHMA3 in wheat greatly decreases Cd accumulation in wheat grain **(Zhang et al. 2020)**. Some members of ATP-binding cassette (ABC) and calcium/H^+ exchanger (CAX) transporters are also involved in the vacuolar Cd sequestration **(Park et al. 2012; Zhang et al. 2016)**. In addition, both enzymatic/non-enzymatic antioxidant defense systems and high-affinity sulfydryl-rich chelators are pivotal for plant Cd resistance through eradicating oxidative impairment and enhancing free-Cd^{2+} chelation, respectively **(Hasanuzzaman et al. 2019; Rahman et al. 2017)**.

Herein, an integrated comparative analysis of phenome, ionome, genome, and transcriptome was performed to dissect the underlying mechanisms differential Cd resistance and grain Cd accumulation in allohexaploid wheat genotypes. Our findings may provide elite gene resources and theoretical basis for the genetic improvement of plant Cd resistance and grain Cd accumulation in wheat and other *Triticum* crop species.

Materials And Methods

Growth conditions and salt treatments

A total of 442 wheat cultivars were hydroponically grown in an illuminated growth chamber using the Hoagland and Arnon nutrient solution **(Zhang et al. 2019)**. The wheat growth conditions was set up as follows: light intensity of 150 μmol m^{-2} s^{-1}, temperature of 22ºC daytime/20ºC night, light period of 16-h photoperiod/8-h dark, and relative humidity of 60% **(Zhang et al. 2018)**.

Root system architecture analysis

After seed germination, uniform wheat plants were grown hydroponically under 10 μM $CdCl_2$ for 14 d. The roots of wheat seedlings were subjected to an image scanner for the analysis of total root length, root volume, root surface area, and average root diameter using WinRHIZO Pro (Regent Instruments, QC, Canada).

Microscopy analysis

Intracellular ultrastructure of leaf pieces (approximately 1 mm^2) from wheat plants, which were treated with 10 μM $CdCl_2$ for 14 d, were determined by a transmission electron microscope (H-7650; Hitachi, Tokyo, Japan). Leaf pieces were also examined by scanning electron microscopy (JSM-6390/LV, JEOL, Tokyo, Japan) to characterize stoma and trichome density. The sample pieces were prepared as described previously **(Dittmer et al. 2021)**. Each test had at least five independent biological replicates.

Determination of total chlorophyll, malondialdehyde, and cell wall components

Chlorophyll pigments were extracted using 80% isopropyl alcohol (v/v), and then the concentrations of purified extracts were determined spectrophotometrically at 663.2, 646.8, and 470 nm **(Hua et al. 2017)**. Likewise, the concentrations of malondialdehyde (MDA), which was extracted using thiobarbituric acid, were assayed spectrophotometrically at the wavelengths of 450 nm, 532 nm, and 600 nm **(Kotula et al. 2020)**. Fractionation and determination of cell wall components were conducted according to the method reported by **Zhang et al. (2019)**.

Determination of reactive oxygen species and antioxidant activity

Fresh leaves and roots were harvested and immediately frozen. Potassium phosphate buffer (pH 7.8) and 0.1% (w/v) trichloroacetic acid were used to obtain the O_2^- and H_2O_2 extracts, respectively. Absorbance of the aforementioned obtained extract was spectrophotometrically determined at the wavelengths of 530 and 390 nm, respectively **(Zhou et al. 2016)**.

The superoxide dismutase (SOD) activity was spectrophotometrically determined at 560 nm using the nitroblue tetrazolium method **(Chu et al. 2016)**. The peroxidase (POD) activity was spectrophotometrically assayed by monitoring the formation of guaiacol at 470 nm **(Fu et al. 2014)**. The catalase (CAT) activity was calculated according to the study by **Aebi (1984)**. The ascorbate peroxidase (APX) activity was assayed according to ascorbate oxidation at 290 nm **(Nakano et al. 1981)**.

Phytohormone assay

Fresh wheat samples were prepared to obtain the phytohormone extract **(Yu et al. 2017)**. The standard auxin (indole-3-acetic acid, IAA), cytokinin (*trans*-zeatin, *t*Z), gibberellin (GA_3), abscisic acid (ABA), jasmonic acid (JA), salicylic acid (SA), and brassinosteroid (BR) were purchased from Sigma-Aldrich (St. Louis, MO, USA) or OlChemIm (OlChemIm, Olomouc, Czech Republic). The phytohormone concentrations were determined by ultra-fast liquid chromatography-electrospray ionization tandem mass spectrometry (UFLC-ESI-MS) **(Liu et al. 2012)**.

Xylem sap collection and ionomic analysis

Xylem sap was collected as described previously **(Kan et al. 2019)**. Wheat plants, treated with 10 μM $CdCl_2$ for 14 d, were cut at 2 cm above the shoot-root junction. The exudates (xylem sap) were collected for 2 h as xylem sap. For this, the leaves were incubated with 5 mM Na_2-EDTA (pH 7.5) for 2 h in a dark high-humidity environment. The collected xylem sap samples were weighed, and then stored at 4°C until further analysis.

Plant tissues and grain powde of wheat, which were treated with 10 μM $CdCl_2$ for 14 d, were over-dried at 65°C to constant weight. To estimate Cd and other cation (including K^+, Ca^{2+}, Mg^{2+}, Fe^{2+}, Cu^{2+}, Mn^{2+}, and Zn^{2+}) concentrations, the fine powder of samples was incubated with an acid mixture (HNO_3:$HClO_4$=4:1, v/v) at 200°C for completed digestion. Ten, to quantify the ion concentrations, the diluted supernatants were subjected to an inductively coupled plasma mass spectrometry (ICP-MS; NexION™ 350X, PerkinElmer) **(Zhang et al. 2019)**.

DNA isolation and whole-genome re-sequencing (WGS)

Genomic DNA from fresh wheat leaves was isolated using 2% CATB. After base calling (Illumina pipeline CASAVA v1.8.2), converted sequence data were subjected to a quality control procedure to remove unusable reads, including adapters, unknown bases, and low-quality reads (quality value ≤ 5). Sequencing reads were aligned to the reference genome using BWA with default parameters. Subsequently, duplicates were removed by SAMTOOLS and PICARD (http://picard.sourceforge.net). Next, the raw SNP and insertion/deletion (InDel) sets identified by samtools were filtered using the following criteria: mapping quality >20 and variate position depth > 4. The function of all assembled unigenes showing polymorphisms between the Cd-resistant and Cd-sensitive genotypes was annotated based on the following databases: Nr (NCBI non-redundant protein sequences), Nt (NCBI non-redundant nucleotide sequences), Pfam (Protein family), KOG (euKaryotic Ortholog Groups), Swiss-Prot (A manually annotated and reviewed protein sequence database), KO (KEGG Ortholog database), and GO (Gene Ontology).The unigenes were annotated in public NR, NT, Swiss-Prot and KOG databases using NCBI blast 2.2.28+, and the Nr, Nt and Swiss-Prot databases had a cut-off E-value of 10^{-5}, while KOG database had a cut-off E-value of 10^{-3} **(Ai et al. 2016).**

The coding sequences and promoter regions of target genes were amplified using the high-fidelity Phusion NEB DNA polymerase. The primers used in this study are listed in **Supplementary Table S1**.

RNA extraction

After seed germination, uniform wheat plants were grown hydroponically under 10 μM $CdCl_2$ for 14 d. Total RNA from fresh wheat tissues was extracted using the Invitrogen TRIzol® Reagent (Invitrogen, CA, USA) following the manufacturer's instructions, and the genomic DNA was removed by TaKara DNase I. RNA quality and quantification was determined by 2100 Bioanalyser (Agilent, CA, USA) using NanoDrop 2000 (Thermo Fisher Scientific, Massachusetts, USA), respectively. Only high-quality RNA samples (OD_{260}/OD_{280}=1.8~2.2, OD_{260}/OD_{230} 3 2.0, RIN ≥ 8.0, 28S:18S ≥ 1.0) were used to construct sequencing libraries.

Library preparation, sequencing, and read mapping

Transcriptome libraries were constructed based on the instructions of TruSeq^{TM} RNA sample preparation Kit (Illumina, San Diego, CA, USA). Briefly, mRNA was isolated based on poly-A selection using the oligo(dT) beads, and was then fragmented. Double-stranded cDNA was synthesized using a SuperScript kit (Invitrogen, CA, USA) with random hexamer primers. Next, the cDNA was subjected to end-repair, phosphorylation, and 'A' base addition according to the Illumina's library construction protocol. 200-300 bp libraries were selected using 2% Low Range Ultra Agarose. After quantification by TBS380 fluorometer, the paired-end (2 × 150 bp) library was sequenced by the Illumina HiSeq Xten system. Raw paired-end reads were trimmed and quality controlled by SeqPrep (https://github.com/jstjohn/SeqPrep) and Sickle (https://github.com/najoshi/sickle) programs with default parameters. Next, clean reads were separately aligned to the reference genome of using TopHat v2.0.0 (http://tophat.cbcb.umd.edu/). The mapping criterion of bowtie was as follows: sequencing reads should be uniquely matched to the genome allowing up to two mismatches, without InDels.

Differential expression and functional enrichment analysis

Expression levels of transcripts were calculated as fragments per kilobase of exon per million mapped reads (FRKM) values via RSEM (http://deweylab.biostat.wisc.edu/rsem/). Both *P*-value and false discovery rate (FDR) < 0.05 were used to identify differentially expressed genes (DEGs). EdgeR (http://www.bioconductor.org/packages/2.12/bioc/html/edgeR.html), was used for differential expression analysis. GO and KEGG enrichment analysis of DEGs was performed by GOATOOLS (https://github.com/tanghaibao/Goatools) and KOBAS (http://kobas.cbi.pku.edu.cn/home.do) at Bonferroni-corrected *P*-value ≤ 0.05 compared with the background whole-transcriptome.

Molecular characterization of candidate genes

The target genes were physically mapped onto wheat chromosomes using MapGene2Chromosome v2.1. Tandem duplicated genes were defined as an array of two or more genes within a 100-kb genomic region **(Smith and Waterman 1987)**. KaKs_calculator was used to calculate the nonsynonymous (Ka) and synonymous (Ks), substitution rates, and Ka/Ks based on the pairwise CDS and amino acid alignment with the yn00 method **(Yang and Nielsen 2000)**. According to the Darwin's evolution theory, it is proposed

that Ka/Ks > 1.0 means positive selection, while Ka/Ks < 1.0 indicates purifying selection, and Ka/Ks = 1.0 denotes neutral selection. Tissue-specific expression profies of the target gene were retrieved from the WheatOmics (http://202.194.139.32/) database **(Ma et al. 2021)**. To identify putative *cis*-acting regulatory elements, two-kb of upstream genomic sequences from the start codon (ATG) of target genes were analyzed by PLACE v. 30.0 (http://www.dna.affrc.go.jp/PLACE/) **(Higo et al. 1999)** and plantCARE (http://bioinformatics.psb.ugent.be/webtools/plantcare/html/) **(Lescot et al. 2002)**.

The *TaHMA2b-7A::GFP* plasmid was constructed by inserting the *TaHMA2b-7A* coding region (without the stop codon) into the KpnI site in the pBI121-GFP vector, which is driven by the CaMV 35S promoter. To assay the role of *TaHMA2b-7* in the Cd resistance, the empty (*pYES2*) and *pYES2-TaHMA2b-7A* plasmids were transformed into INVSc1 yeast cells using the lithium acetate method **(Tan et al. 2013)**. Subcellular localization of *TaHMA2b-7A* was obtained using PEG-mediated protoplast transformation in rice **(Voelker et al. 2006)**. Fluorescence was observed using a Nikon C2-ER confocal laser scanning microscope (Nikon, Japan) following emission filter sets at 510 nm (GFP) and 580 nm (RFP), and excitation was achieved at 488 nm (GFP) and 561 nm (RFP). The fluorescent dye FM4-64 was used as the maker of plasma membrane-localization **(Zhang et al. 2017)**.

Reverse transcription-quantitative polymerase chain reaction (RT-qPCR) assays

RT-qPCR assays were performed to examine the relative expression of target genes. After removing genomic DNA using RNase-free DNase I, total RNA was used as RT templates for cDNA synthesis using the TaKaRa PrimeScript^{TM} RT Reagent Kit Eraser. The RT-qPCR assays were conducted using TaKaRa SYBR®*Premix Ex Taq*^{TM} II under a Bio-Rad's C1000 touch Thermal Cycler of CFX96^{TM} Real-time PCR detection System.

The thermal regime was as follows: 95ºC for 3 min, 40 cycles of 95ºC for 10 s, and 60ºC for 30 s. The melt curve was plotted according to the following PCR procedure: 95ºC for 15 s, 60ºC for 1 min, and 60-95ºC for 15 s (+0.3ºC/cycle). The gene expression levels were calculated with the $2^{-\Delta\Delta C}{}_{T}$ method **(Livak and Schmittgen 2001)** using as the internal reference. The primers used in this study are listed in **Supplementary Table S1**.

Statistical analysis

The Statistical Productions and Service Solutions 17.0 (SPSS, Chicago, IL, USA) was used to perform statistical tests. The Student' *t* test or one-way analysis of variance (ANOVA), followed by Tukey's honestly significant difference multiple comparison tests, was used to determine the significant differences.

Results

Natural variations in Cd resistance and morpho-physiological characterization of wheat genotypes

To identify genotypic differences regarding Cd resistance among natural wheat genotypes, a panel consisting of 442 cultivars were grown under 10 μM $CdCl_2$ for 14 d using hydroponic culture system, and the chlorotic spots of leaves was used as a proxy for Cd resistance. It was observed that maximal lengths of leaves and roots ranged from 5.0 cm to 38.8 cm (with the variance coefficient of 27.2%) and from 6.0 cm to 33.6 cm (with the variance coefficient of 27.3%), respectively **(Fig. 1A and 1B)**. Based on wide natural variation in Cd resistance occurring among different wheat genotypes, the lengths of chlorotic leaves caused by Cd toxicity were further investigated to identify the most sensitive wheat genotypes. The results showed that the chlorotic leaf lengths ranged from 1.83 cm to 15.8 cm, with the variance coefficient of 13.3% **(Fig. 1C).** Based on these investigations,

Next, to examine the biological basis of these natural variations, we selected ‘Zhengmai 1860’ (‘ZM1860’) and ‘Zhoumai 32’ (‘ZM32’) as the most Cd-resistant and Cd-sensitive wheat genotypes for the subsequent analysis. Under Cd-free (control) conditions, the two wheat genotypes showed no marked differences in growth performance **(Fig. 1D)**. However, ‘ZM32’ showed obvious plant lodging compared with ‘ZM1860’ under Cd toxicity **(Fig. 1D).** After exposure to 10 μM Cd for 14 d, the leaves of ‘ZM32’ showed severe chlorosis than those of ‘ZM1860’, which showed few significant differences with the plants under control **(Fig. 1E)**. Moreover, the roots of ‘ZM32’ also showed significant inhibition **(Fig. 1F).** To be accurate, the dry biomasses of shoots and roots of ‘ZM1860’ were 73.53% and 124.4% higher than those of ‘ZM32’ under Cd toxicity **(Fig. 1G, H)**. Further, we also found that the ratio of root/shoot was significantly higher in ‘ZM1860’ than in ‘ZM32’ **(Fig. 1I)**. In terms of the leaf morphology, both maximal leaf lengths and total leaf areas were tested to be 21.67% and 65.90% higher in ‘ZM1860’ than in ‘ZM32’ **(Fig. 1J, K)**. However, the leaf angles of ‘ZM32’ were significantly larger than those of ‘ZM1860’ **(Fig. 1L)**, the leaves of whichshowed significantly higher chlorophyll concentrations **(Fig. 1M)**.In terms of the root system architecture, all of the maximal root lengths **(Fig. 1N)**, root surface areas **(Fig. 1O)**, root volumes **(Fig. 1Q)**, root tip numbers and **(Fig. 1R)** were markedly larger in ‘ZM1860’ than in ‘ZM32’ **(Fig. 1N-R)**. However, average root diameters were not identified to be significantly different between the two wheat genotypes **(Fig. 1N).**

To examine the cellular effects underlying the morphological differences, we characterized the leaf ultrastructure using electron microscopy. The stoma density were highly similarly between ‘ZM1860’ and ‘ZM32’ under both control and Cd conditions **(Fig. 2A-E)**, whereas the trichome density of ‘ZM1860’ was significantly higher than that of ‘ZM32’ under Cd toxicity **(Fig. 2J)**. Further, TEM analysis showed that the cell morphology of ‘ZM1860’ under Cd toxicity remained similar to that under Cd toxicity **(Fig. 2F, H)**; in contrast, more leaf detached cells in leaves were examined in ‘ZM32’ than in ‘ZM1860’ **(Fig. 2G, I)**. Moreover, more complete chloroplasts with better grana were identified in the leaf mesophyll cells of ‘ZM1860’ compared with ‘ZM32’ **(Fig. 2K-O).**In addition, we also found that ‘ZM1860’ had much thicker cell walls than did ‘ZM32’ under Cd toxicity although no obvious differences were tested between the genotypes under control condition **(Fig. 2P-T).** Further analysis of cell wall components showed that the shoot lignin concentration of ‘ZM1860’ was 17.91% higher than that of ‘ZM32’ **(Figure S1E)** although the concentrations of cellulose, semi-cellulose, and pectin were highly similar between the two wheat

genotypes under Cd **(Figure S1A, C, G)**. Meanwhile, we also investigated their cell wall components in the roots. A significantly higher pectin concentration was observed in 'ZM32' than in 'ZM1860' **(Figure S1H)** whereas the three other components did not differ between 'ZM1860' and 'ZM32' **(Figure S1B, D, F)**.

Differential ROS and phytohormone homeostasis in wheat genotypes

Significantly higher concentrations of MDA, an indicator of membrane lipid peroxidation, were found in 'ZM32' than in 'ZM1860' under Cd toxicity **(Fig. 3A, B)**. The pivotal role of sulfydryl in Cd detoxification led us to test the GSH differences between the Cd-resistant and Cd-sensitive genotypes. The result revealed a significantly higher of GSH in the shoots of 'ZM32' than in the shoots of 'ZM1860' **(Fig. 3C)** whereas obvious differences were not observed in the roots **(Fig. 3D)**.

To identify the ROS catabolism differences between the wheat genotypes under Cd toxicity, we tested the ROS levels and antioxidant enzyme activity. The results showed that both H_2O_2 and O_2^- had obviously higher levels in 'ZM32' than in 'ZM1860' **(Fig. 3E-H)**, particularly in the roots of these two wheat genotypes **(Fig. 3F, H)**. Further DAB and NBT staining confirmed the ROS over-accumulation in 'ZM32' relative to 'ZM1860' **(Fig. 3I, J)**. Subsequently, the activity assays of antioxidant enzymes showed that different antioxidant enzymes showed distinct roles in the ROS homeostasis between shoots and roots. To be specific, the CAT, APX, and GPX enzymes presented significantly higher activity in the shoots of 'ZM32' than in the shoots of 'ZM1860' **(Fig. 3K-T)**. However, we found that 'ZM1860' had much higher activity ofbothSOD and CAT in the roots **(Fig. 3K-T)**.

Although several phytohormones were found to be different between the Cd-resistant and Cd-sensitive genotypes under control **(Fig. 3U)**, more attention was paid to their differences in these two genotypes under Cd toxicity. In the shoots, an obviously higher concentration of SA was observed in 'ZM32' than in 'ZM1860' whereas no significant differences were not identified in other six phytohormones **(Fig. 3U)**. In the roots, both IAA and GA_3 showed markedly higher levels in 'ZM1860' than in 'ZM32', whereas the concentrations of ABA and JA in 'ZM32' were almost twice of those in 'ZM1860' **(Fig. 3U)**.

Ionomic basis of differential plant Cd resistance in wheat genotypes

Based on the significant morpho-physiological differences between the Cd-resistant and Cd-sensitive genotypes, ICP-MS was employed to reveal the ionomic basis of differential Cd resistance**.** Firstly, total Cdconcentrations of whole plants were found to be significantly higher in 'ZM1860' than in 'ZM32' **(Fig. 4A)**, whereas 'ZM1860' accumulated 47.75% of Cd higher than 'ZM32' in whole plants **(Fig. 4B)**. Furthermore, the Cd concentration of whole shoots was significantly higher in 'ZM1860' than in 'ZM32' **(Fig. 4C)**. Further, we tested the Cd concentrations at different positions of leaves, and the Cd concentrations were gradually decreased from mature leaves to young leaves in both 'ZM1860' and 'ZM32' **(Fig. 4D)**. Moreover, the Cd concentration of each leaf was significantly higher in 'ZM1860' than in 'ZM32' **(Fig. 4D)**. Subsequently, we found that the root Cd concentration of 'ZM32' was 25% higher than that of 'ZM1860' **(Fig. 4E)**. Based on the plant biomasses and Cd concentrations above, both shoot and root content were obtained. The results showed that more Cd was accumulated in the shoots of 'ZM1860'

than in the shoots of ‘ZM32’ **(Fig. 4F)**, which had a higher content of root Cd than ‘ZM1860’ did **(Fig. 4G)**. This differential Cd allocation led to a higher translocation coefficient of Cd from roots to shoots in ‘ZM32’ than in ‘ZM1860’ **(Fig. 4H)**. To further characterize the differential long-distance translocation of Cd, the vascular Cd concentrations were determined. The results showed that the Cd concentrations in the stems and xylems of ‘ZM32’ were more than twice and 1.5-fold of those in ‘ZM1860’ **(Fig. 4I, J)**.

To further identify the differential long-distance translocation of Cd between the Cd-resistant and Cd-sensitive genotypes, the grains were harvested at the maturity stage of wheat plants that were grown under 10 μM Cd condition. Although obvious significant differences were not in the grain appearances between ‘ZM1860’ and ‘ZM32’ **(Fig. 4K),** a significant higher Cd concentration was identified in the grains of ‘ZM32’ than in the grains of ‘ZM1860’ **(Fig. 4L)**. Moreover, we also found that the ‘ZM1860’ grains had much higher concentrations of K, Mg, Fe, Cu, Mn, and Zn than ‘ZM32’ did **(Fig. 4M, O, P, Q, R, S)** except for a higher level of grain Ca in ‘ZM32’ than in ‘ZM1860’ **(Fig. 4N).**

WGS-based identification of genomic variations between Cd-resistant and Cd-sensitive genotypes

To identify genomic variations between the Cd-resistant and Cd-sensitive genotypes, we performed deep WGS of both ‘ZM1860’ and ‘ZM32’, generating 170.5 Gb (about 10.21 ×) 192.5 Gb (about 11.51 ×) clean data for ‘ZM32’ and ‘ZM1860’, respectively **(Supplementary Table S2)**. The high-quality sequencing parameters, including Q_{20} and Q_{30}, were ≥ 92%, and the mapping and coverage rates of WGS data were ≥ 98% and ≥ 95% for these two genotypes, respectively **(Supplementary Table S2)**. Such a broad coverage and read depth validated the high quality of genome assembly and sequencing data.

As shown in **Fig. 5**, thousands of genomic variants, including SNPs and InDels, between ‘ZM32’ and ‘ZM1860’, were randomly distributed across the 21 chromosomes of allohexaploid wheat. In total, 14,833,473 SNPs were identified across the 21 chromosomes of wheat **(Fig. 5A)**, ranging from 30,532 (Chr. 6D) to 3,088,362 (Chr. 3B) with an average of 674,289 SNPs on each chromosome **(Fig. 5A, B)**. Strong differences were observed in terms of SNP proportions among the A, B, and D subgenomes, with the B subgenome being the more polymorphic (8,109,845 SNPs; 54.67%), followed by the A-genome (5,779,020; 38.96%) then the D-genome (816,689; 5.507%) **(Fig. 5B)**. The frequency of SNPs on each chromosome varied from 1 per 24,585 bp (Chr. 6D) to 1 per 241 bp (Chr. 3B), with an average value of 1 per 3,967 bp **(Fig. 5B)**. The nucleotide diversity π (average SNP number per nucleotide) ranged from 4.00 × 10^{-5} (Chr. 6D) to 4.15 × 10^{-3} (Chr. 3B), with an average value of 1.27 × 10^{-3}, 1.74 × 10^{-3}, and 1.90 × 10^{-4} on the A, B, and D subgenomes, respectively **(Fig. 5C)**. The annotations of reference (‘Chinese Spring’) genome were used to examine the distribution of SNPs within various genomic features. Among the genome-wide 14,833,473 SNPs between the Cd-resistant and Cd-sensitive genotypes, 71.04% of SNPs belonged to the transition type (A/G and C/T; Ts), which was more than that 28.96% of the trans-versions (A/C, A/T, C/G and G/T; Tv) **(Supplementary Figure S2A)**. This led to an average Ts/Tv ratio of 2.45 **(Supplementary Figure S2A)**, a value that is similar to what has been reported previously in wheat **(Rimbert et al., 2018)**. There was 1.424% of the total SNPs detected in the genic regions (including exonic, intronic, and splicing regions), whereas a much larger proportion of SNPs (98.576%) were located in the

2.0-kb upstream (promoter), 1.0-kb downstream, and other intergenic regions **(Supplementary Fig. S2B)**. Among the SNPs located in the genic areas, 40.38% of the variations occurred in the coding sequences **(Supplementary Fig. S2B)**. Only a minor fraction (1.01%) of the SNPs located in the exonic regions were mapped onto the stop codons **(Supplementary Fig. S2C)**. In general, the ratio of synonymous SNPs (46.62%) to non-synonymous SNPs (52.37%) was about 0.89 **(Supplementary Fig. S2C)**.

Also, a total of 1,147,284 InDels were identified that were unevenly distributed over the wheat genome **(Fig. 5D)**, ranging from 7,265 (Chr. 4D) to 183,650 (Chr. 3B) with an average of 54,633 InDels on each chromosome **(Fig. 5D, E)**. The majority (97.6%) of total InDel variants occurred in the 2.0-kb upstream (promoter), 1.0-kb downstream, and other intergenic regions, whereas a little proportion (2.40%) of InDels were identified in the genic sequences **(Supplementary Fig. 3A)**. Among the InDels occurring in the exons, only ~1.64% were identified in the stop codons. For the other InDels, 47% of SNPS caused frame-shift deletion or insertion **(Supplementary Fig. 3B)**. In terms of the InDel length variation occurring in the genomic or genic regions, the mono-nucleotide type was the most **(Supplementary Fig. 3C, D)**.

Based on the annotation results shown in **Fig. 6A**, there were 117,861 unigenes (94.70%)

annotated in NR, 117,090 unigenes (94.08%) annotated in Nt, 36,445 unigenes (29.28%) annotated in KO, 82,499 unigenes (66.28%) annotated in SwissProt; 84,666 unigenes (68.02%) annotated in PFAM; 84,661unigenes (68.02%) annotated in GO; 23,499 unigenes (18.88%) annotated in KOG. In summary, there were 15,305 unigenes (12.29%) annotated in all databases, and 122,930 unigenes (98.77%) annotated in at least one database.

KOG, GO, and KEGG are international standardized systems of gene functional classification that describe properties of genes and their products in any organism. The genome-wide unigenes with polymorphisms between the Cd-resistant and Cd-sensitive genotypes were categorized into 26 groups of KOG function clusters, among which the ‘general function prediction only’ cluster had the highest number (3,396; 14.45%) of unigenes, whereas the small clusters of ‘cell wall/membrane/envelope biogenesis’, ‘inorganic ion transport and metabolism’, and ‘defense mechanisms’ were paid more attention **(Fig. 6B)** due to their close relationships with Cd resistance. Regarding the GO analysis, the genome-wide DNA variants were found to be accumulated in the terms involving detoxification, response to stimulus, antioxidant activity, and transporter activity **(Fig. 6C)**. In terms of the KEGG analysis, revealed that the pathways were identified to be implicated in processes of environmental adaptation, signaling transduction, membrane transport, transport and catabolism, and cell growth and death **(Fig. 6D)**.

Transcriptomics-based variations between Cd-resistant and Cd-sensitive genotypes

Based on the morpho-physiologic, ionomic, and genomic differences, to further identify the DEGs regulating differential Cd resistance in wheat genotypes, a high-throughput genome-wide transcriptome sequencing was performed for both ‘ZM32’ and ‘ZM1860’. After removing adapter sequences and low-quality reads, approximately 4.7×10^7 clean reads were obtained from each sample. The total length of clean reads from the 24 samples reached about 1.67×10^{10} nt with $Q_{20} > 97\%$ and $Q_{30} > 93\%$, and the

mapping rate of all samples were more than 90% **(Supplementary Table S3)**. Taken together, these parameters indicated that the transcriptome sequencing data were of high quality suitable for the following analysis.

Principal component analysis showed that compared with the control, the two genotypes and their tissues exhibited significantly different transcriptomic features under Cd toxicity **(Fig. 7A)**, which indicated genotype- and organ-specific transcriptomic responses to Cd toxicity. Further, *Pearson* correlation coefficients between each RNA-seq group showed that the same organs (shoots/roots) had much higher correlation than the same treatments (control/Cd) irrespective of 'ZM1860' or 'ZM32' **(Fig. 7B)**. In both shoots and roots, more Cd-responsive DEGs were identified in 'ZM32' than in 'ZM1860' **(Fig. 7C)**. Moreover, a larger number of DEGs between 'ZM1860 and 'ZM32' were found in both shoots and roots, and the DEGs had higher expression levels in 'ZM32' than in 'ZM1860' under both control and Cd conditions **(Fig. 7D).** Venn diagram analysis showed that 192 and 1,776 genes responsive to Cd toxicity were differentially expressed in the shoots and roots between 'ZM1860' and 'ZM32' **(Fig. 7E, F)**, and some of these 1,776 DEGs were presumed to be the core regulators responsible the differential long-distance translocation of Cd from roots to shoots. GO enrichment analysis revealed that the Cd-responsive DEGs in the shoots were mainly involved in the categories of active transmembrane transporter activity, oxidoreductase activity and ATPase **(Fig. 7G)**. KEGG analysis showed that the metabolism of fatty acid, ascorbate, sulfur (cysteine, methionine, and glutathione), and phytohormone signal transduction were over-represented under Cd toxicity **(Fig. 7H).**

Identification of core Cd transporter family members regulating differential Cd resistance

The differential ionomic profiling indicated that less root xylem Cd translocation causing a lower shoot Cd concentration, was the key factor for Cd resistance in 'ZM1860' relative to 'ZM32' **(Fig. 4)**. Although many transporters are reported to be involved in the Cd resistance and detoxification, HMA2/4s have been the only two transporters essential for root-to-shoot Cd translocation to counter Cd toxicity in plants **(Li et al. 2014)**. Based on these findings, we defined the candidate genes, responsible for differential wheat Cd resistance, as the DEGs only in the roots.

Among the nine *TaHMA* (*HMA1-HMA9*) subfamilies, only six of them were identified to be expressed in this study **(Fig. 8A)**. Both HMA2 and HMA4 have a single member in both Arabidopsis ad rice, namely AtHMA2/OsHMA2 and AtHMA4/OsHMA4 **(Berthomieu et al. 2003)**. However, all of the genome-wide six *TaHMA2s* and three *TaHMA4s* were identified in this study, however, we only examined the differential expression of *TaHMA2b-7A* (TraesCS7A02G420000) and *TaHMA2b-7B* (TraesCS7B02G320900) in the roots under Cd toxicity **(Fig. 8A)**. Given the fact that the Cd-sensitive genotype 'ZM32' had a higher translocation coefficient of Cd from roots to shoots than 'ZM1860' did, therefore, *TaHMA2b-7B* was excluded from the two candidate genes due to its higher expression in 'ZM1860' than in 'ZM32'. In summary, *TaHMA2b-7A* was proposed to be the key candidate responsible for differential Cd resistance between these two wheat genotypes. A genome-wide association analysis of a natural population consisting 206 wheat genotypes was performed based on the maximal root length under Cd toxicity, and

we also found that the *TaHMA2* homologs, including *TaHMA2b-7A*, were located in the candidate genomic regions for natural variations in Cd resistance **(Fig. 8B)**.

Molecular characterization of *TaHMA2b-7A*

Subsequently, more in-depth analysis was conducted to characterize the molecular function of *TaHMA2b-7A* and the possible reasons for its differential expression between the Cd-resistant and Cd-sensitive genotypes. Gene sequence analysis showed that the full-length genomic region, including nine exons and eight introns, of *TaHMA2b-7A* was 6,535 bp, encoding 939 amino acids **(Fig. 8C)**. WGS and PCR-based gene cloning showed that sequence differences were not identified in the exon regions, which led to identical amino acid sequences between 'ZM1860' and 'ZM32'. Further sequence polymorphism analysis revealed a 25-bp deletion ($^{-697}$GTGTGGCCCATGAATTCTAGGTACA^{-721}) in the *TaHMA2b-7A* promoter region of 'ZM32' compared with 'ZM1860' **(Fig. 8D)**. *Cis*-acting regulatory element analysis showed that a core Cu-responsive element ($^{-716}$GTAC^{-720}) existed within the InDel site (**Supplementary Table S4**), which might be the major reason for the differential expression of *TaHMA2b-7A* in the Cd-resistant and Cd-sensitive genotypes.

In addition to eight transmembrane domains with a very long C-terminal region **(Fig. 8E)**, the conserved motifs of N-terminal metal-binding (GICCPSE), phosphatase (TGES), ion translocation (CPC), aspartyl phosphate formation (DKTGT), and ATP-binding (GDGMNDA) were also identified in the amino acid sequences of TaHMA2b-7A **(Fig. 8F)**. Within the N-terminal metal-binding domain (GICCPSE), the two cysteine residues determining the HMA activity and affinity with metal substrates **(Wong et al. 2009)**, were identified in TaHMA2b-7A, OsHMA2, and AtHMA2 **(Fig. 8F)**. To further characterize the evolutionary pattern of *TaHMA2b-7A*, the six *HMA2* homologs were physically mapped onto the wheat chromosomes **(Fig. 8G)**. We found that the physical distances within both the *TaHMA2a-7A* and *TaHMA2b-7A* pair and the *TaHMA2a-7D* and *TaHMA2b-7D* pair were smaller than 100 kb **(Fig. 8G)**, which indicated these four *HMA* homologs were formed as a result of tandem duplication, whereas the other two homologs (*TaHMA2a-7B* and *TaHMA2b-7B*) arose from segmental duplication. Evolutionary selection pressure analysis revealed that the non-synonymous (Ka)/synonymous (Ks) nucleotide substitution rate (0.85) of *TaHMA2b-7A* was < 1.0 **(Fig. 8H)**, which suggesting a purifying selection to preserve its function. Furthermore, subcellular localization analysis showed that TaHMA2b-7A was localized in the plasma membrane **(Fig. 8I)**.

Phylogeny analysis showed that the HMA2 homologs of diverse plant species were obviously classified into two clades: monocots and dicots **(Fig. 9A)**, and this suggested the evolutionary divergence of HMA2s occurred after plant speciation. Functional studies and phylogeny analysis of HMAs have shown that these transporters can be divided into three subgroups based on their metal-substrate specificity: (i) a Cu/Ca/Zn/Cd/cobalt (Co) group, (ii) a Zn/ Co/Cd/lead (Pb) group, and (iii) a Cu group (**Hermand et al. 2014**; **Fig. 9B**), and all of AtHMA2, OsHMA2 and TaHMA2b-7A were clustered within the Zn/ Co/Cd/Pb-ATPase clade **(Fig. 9B)**. Then, we investigated the spatio-temporal expression patterns of *TaHMA2b-7A* **(Fig. 9C-H)**. After exposure to 12-h Cd toxicity, the *TaHMA2b-7A* expression was dramatically increased

until 1 d, and its expression was kept steadily from 1-d to 5-d Cd toxicity, which showed periodic increase-steadiness changes **(Fig. 9C)**. In general, the *TaHMA2b-7A* expression showed an increased trend with the solution Cd concentrations increasing **(Fig. 9C)**. In addition to the transcriptional response of *TaHMA2b-7A* to Cd toxicity, we also examined the *TaHMA2b-7A* expression under low Fe, low Zn and salt stress**.** The results showed that *TaHMA2b-7A* was induced by the three nutrient stresses, particularly in the roots **(Fig. 9E-G)**. Therefore, it led us to investigate the growth performance of the Cd-resistant 'ZM1860' and Cd-sensitive 'ZM32'under low Fe and low Zn stresses. The results showed that 'ZM1860' presented higher resistance to low Zn but sensitivity to low Fe (**Supplementary Fig. S4**).

To further explore the roles of *TaHMA2b-7A* in the growth and development of wheat plants, we tested its expression at the stages of seedlings, tillering, flag leaves, booting, anthesis, grain filling and ripening. The expression profiling showed that at the stages of both tillering and flag leaf, *TaHMA2b-7A* showed relatively higher expression in the roots; however, when wheat plants enter the reproductive stages, *TaHMA2b-7A* wasmainly expressed in the internodes, spikelets, and grains **(Fig. 9H)**.

Natural variations of *TaHMA2b-7A* in regulating wheat Cd resistance

To further understand the pivotal roles of *TaHMA2b-7A* in regulating wheat Cd resistance, an association analysis between their differential expression and wheat Cd resistance was performed in 14 wheat cultivars randomly selected from our collected wheat resources, including 'ZM1860' and 'ZM32'. Based on the Cd resistance assessment, 'ZM1860' and other six cultivars ('Lunxuan 715', 'Zheng 103', 'Shannongtedali 1', 'Zhongyuan 6', 'Fengdecun 5', and 'Xinmai 19') were identified to be Cd-resistant with less leaf chlorosis under Cd toxicity **(Fig. 10A, B)**, whereas 'ZM32' and other xin cultivars ('Yangmai 20', 'Zengmai 518', 'Jingdong 1', 'Zhengmai 369', 'Han 6172', and 'Ruiquanmai 24') were rated with high Cd sensitivity with more severe leaf chlorosis **(Fig. 10A, B)**. In general, the chlorotic lengths of leaves in the seven Cd-sensitive genotypes were significantly larger than those in seven Cd-resistant genotypes **(Fig. 10C).** Further,we examined the Cd concentration in both shoots and roots of the 14 wheat genotypes, and calculated the translocation coefficients of Cd from roots to shoots. On the whole, the Cd-sensitive genotypes allocated a larger proportion of Cd to the shoots than the Cd-resistant genotypes did **(Fig. 10D)**. *TaHMA2b-7A* showed significantly higher expression levels in the seven Cd-sensitive genotypes than in the seven Cd-resistant genotypes **(Fig. 10E).** Moreover, the leaf chlorosis of wheat plants was positively correlated with the *TaHMA2b-7A* expression under Cd toxicity **(Fig. 10F).**

Discussion

Integrated multi-omics analysis provided rapid and effective ways to reveal key mechanisms underlying Cd resistance and accumulation in allohexaploid wheat

Recent high-throughput techniques, such as next-generation sequencing, have generated numerous multi-omics datasets to enable the rapid and efficient dissection of biological functions and mechanisms via multiple facets **(Nguyen and Wang 2020)**. Cost reductions in high-throughput sequencing and advances in sequence assembly algorithms have eased the identification of core genetic and molecular

mechanisms underlying key agronomy traits even in plant species with large and complex or polyploid genomes **(Jayakodi et al. 2021)**.

Polyploidy events resulted in numerous duplicated segments and homeologous regions within the wheat genome (AABBDD) that has more than 120 thousand genes (**IWGSC et al. 2018)**. In allohexaploid wheat, homologous sequences from different chromosomes and their interactions present huge difficulty in dissecting biological mechanisms under key agronomy traits. In this study, an integrated analysis of comparative phenome, ionome, WGS, RNA-seq, and association analysis was examined to reveal the core mechanisms underlying differential plant Cd resistance and grain Cd accumulation in wheat. Firstly, a large number of wheat cultivars collected provided wide natural variations in plant Cd resistance for us to further select the genotypes with extreme Cd resistance and sensitivity. Phenome, including the characterization of RSA, ultrastructure, cell wall components, ROS homeostasis and phytohormone profiling, enriched our understanding of the physiological responses of wheat plants to Cd toxicity.

The plant cell wall is the first barrier to touch environmental Cd, which disrupts cell wall biogenesis and organization **(Hu et al. 2021)**. This study found that Cd toxicity induced very severe lodging of the Cd-sensitive genotype (**Figs. 1 and 2**), and this was presumed to be related to the disorder of cell wall components, particularly lignin. In addition, what was more noteworthy that obvious increase in the ABA, SA, and JA concentrations but lower IAA and GA_3 levels in 'ZM32' than in 'ZM1860' (**Fig. 3U**), and the phytohormone changes might be closely related to Cd-induced leaf chlorosis and root growth retardation. These findings would point out the direction of genetic improvement of plant Cd resistance and accumulation.

Then, the ionomic signatures showed that it is long-distance translocation of Cd is the determinant factors that regulated the differential Cd resistance, which defined the HMA2/4 homologs as the candidate genes without quantitative trait locus (QTL) mapping or genome-wide association analysis. Finally, transcriptome sequencing-based identification of DEGs together with WGS-assisted characterization of sequence polymorphisms pointed out that a *HMA2* homolog controlled the differential root-to-shoot Cd translocation. Next, we would like to use the Cd-resistant and Cd-sensitive genotypes as the parents to construct doubled haploid populations or recombinant inbred lines, and perform map-based cloning of QTLs for wheat Cd resistance and grain Cd accumulation in wheat in the next work.

Long-distance Cd translocation regulate Cd resistance and accumulation in plants

A previous study showed that rapeseed genotypes with higher nitrogen use efficiency show weaker vacuolar nitrate sequestration and stronger root-to-shoot nitrate transport than the nitrogen-inefficient genotypes do **(Han et al. 2016)**. Low nitrate is identified to alleviate Fe deficiency through promoting root-to-shoot transport of Fe in apple **(Sun et al. 2021)**. Our previous study also revealed that xylem sodium unloading-mediated long-distance translocation is essential for plant salinity resistance **(Zhou et al.**

2021). Therefore, it can be concluded that root-to-shoot ion translocation is very pivotal for efficient nutrient use and stress resistance in crop species.

In this study, the ionomic profiling suggested that in contrast to the Cd-sensitive genotype, the Cd-resistant genotype had a lower shoot Cd concentration **(Fig. 3C)**, which countered severe Cd toxicity and maintained shoot photosynthesis. Lower stem and root xylem Cdconcentrations ensured a higher proportion of Cd in the roots of 'ZM1860' than in the roots of 'ZM32' **(Fig. 3I, J)**. This finding suggested that long-distance translocation of Cd from roots to shoots is the fundamental reason for the differential Cd resistance in wheat genotypes. Moreover, we also found that a lower shoot Cd concentration finally resulted in a lower Cd concentration in wheat grains of 'ZM1860' **(Fig. 3L)**, which not only showed stronger plant Cd resistance but also accumulated fewer Cd and more micronutrients in grains. The transcriptional profiling of the candidate gene *TaHMA2b-7A* at the whole stages **(Fig. 9H)** indicated that *TaHMA2b-7A* might be mainly responsible for Cd translocation from roots to shoots at the vegetative stage, whereas it might be involved in Cd influx into grains at the reproductive stage. Considering that 'ZM1860' is a wheat cultivar with elite agronomy traits, we proposed 'ZM1860' as a promising wheat cultivar widely grown in soils with Cd contamination.

Potential functional analysis and transcriptional regulation of TaHMA2b-7A

In this study, analysis of phylogeny and conserved motifs indicated that TaHMA2b-7A, similar to AtHMA2 and OsHMA2, might have the transport activity of Cd, Fe, and Zn. However, TaHMA2b-7A had eight potential transmembrane domains (**Fig. 8E**); this result was similar to that of AtHMA2 **(Wong et al. 2009)** but different from that of OsHMA2, which has six transmembrane domains **(Satoh-Nagasawa et al. 2012)**. Our data showed that TaHMA2b-7A was a plasma membrane-localized Cd exporter that might pump Cd into the apoplast and exhibited functions similar to those of AtHMA2 **(Wong et al. 2009)** and OsHMA2 **(Satoh-Nagasawa et al., 2012; Takahashi et al. 2012)** as previously reported. Nevertheless, *HMA2* in *Hordeum vulgare* confers Cd sensitivity to wild-type yeast **(Mills et al. 2012)**.

Under Cd toxicity, low Fe, and low Zn stresses, the *TaHMA2b-7A* expression was consistently increased **(Figs. 8A, 9C, E, F)**. However, the expression of *AtHMA2* was reported to be not changed when exposed to various metals, including Zn and Cd (**Eren and Arguello 2004**). The *OsHMA2* expression was found to be decreased in the roots under Zn deficiency, whereas under Cd toxicity, its expression levels were unchanged **(Takahashi et al. 2012**), increased **(Nocito et al. 2011)** or decreased **(Ogawa et al. 2009)**. This inconsistency might be attributed to two major reasons: (i) the use of different cultivars and Cd/Zn treatment conditions (including treatment time and media concentrations, among others) in the same plant species; (ii) different transcriptional regulatory mechanisms of *HMA2s* in different species.

In this study, *TaHMA2b-7A* was thought to be mainly responsible for Cd resistance of 'ZM1860' and Cd sensitivity of 'ZM32' with higher *TaHMA2b-7A* expression, which caused a larger proportion of Cd translocation from roots to shoots. An InDel site within the promoter region might lead to differential expression of *TaHMA2b-7A*, and a core Cu-responsive element ($^{-716}$GTAC^{-720}) was identified within the

InDel site (**Supplementary Table S4**). However, the transcriptional or other pathway regulation of HMAs is scarcely reported in Arabidopsis and rice as yet, not to mention those in wheat and other crop species with vast and complex genomes. Therefore, the roles of the core Cu-responsive element and other potential components in the transcriptional regulation of *TaHMA2b-7A* and other *HMA* homologs needs to be further explored in the near future.

Abbreviation

Cd, cadmium;

DEG, differentially expressed gene;

GO, gene ontology;

HMA, heavy metal ATPase;

InDel, insertion/deletion;

KEGG, Kyoto Encyclopedia of Genes and Genomes;

MDA, malondialdehyde;

RSA, root system architecture;

RT-qPCR, reverse-transcription quantitative polymerase chain reaction;

SNP, single nucleotide polymorphism;

Ta, *Triticum aestivum*;

WGS, whole-genome re-sequencing.

Declarations

Funding

This study was financially supported by the National Natural Science Foundation of China (31801923), National Key R&D Program of China (2021YFD1700900), Natural Science Foundation of Hunan Province (2019JJ50246), Key Science and Technology Project of Henan Province (202102110006), Innovation Ecosystem Construction Science and Technology Special Project of National Supercomputing Zhengzhou Center (201400210600), Major Collaborative Innovation Project of Zhengzhou City (Key Discipline Construction Project of Zhengzhou University) (NO. xkzdjc201905), and Youth Innovation Project of Key discipline of Zhengzhou University (NO. XKZDQN202002).

Competing interest

The authors have no relevant financial or non-financial interests to disclose.

Author contributions

All authors contributed to the study conception and design. Ying-peng Hua, Ting Zhou, and Jin-yong Huang conceptualized the project and were responsible for acquiring the funding; Ying-peng Hua, Ting Zhou, Jun-fan Chen, and Dan-dan Shen performed the experiments; Ying-peng Hua, Cai-peng Yue, and Ting Zhou analysed and interpreted the data; Shao-min Huang and Zheng-fu Zhou provided some experimental materials; Ying-peng Hua wrote the paper with significant input from all other authors. All authors read and approved the final manuscript.

Data availability

The datasets generated during and/or analysed during the current study are available from the corresponding author on reasonable request.

Ethics approval

The authors declare that the experiments comply with the current laws of the country in which they were performed.

References

1. Abedi T, Mojiri A (2020) Cadmium uptake by wheat (*Triticum aestivum* L.): an overview. Plants (Basel) 9:500
2. Aebi H. Catalase in vitro, vol. 105. New York: Academic; 1984.
3. Ai Y, Zhang Q, Wang W, Zhang C, Cao Z, Bao M, He Y (2016) Transcriptomic analysis of differentially expressed genes during flower organ development in genetic male sterile and male fertile *Tagetes erecta* by digital gene-expression profiling. PLoS One 11:e0150892
4. Amin I, Rasool S, Mir M, Wani W, Masoodi K, Ahmad P (2020) Ion homeostasis for salinity tolerance in plants: a molecular approach. Physiol Plant 171:578-594
5. Baxter I, Tchieu J, Sussman MR, Boutry M, Palmgren MG, Gribskov M, Harper JF, Axelsen KB (2003) Genomic comparison of p-type ATPase ion pumps in Arabidopsis and rice. Plant Physiol 132: 618–628
6. Chu M, Chen P, Meng S, Xu P, Lan W (2021) The Arabidopsis phosphatase PP2C49 negatively regulates salt tolerance through inhibition of AtHKT1;1. J Integr Plant Biol 63:528-542
7. Chu XT, Fu JJ, Sun YF, Xu YM, Miao YJ, Xu YF, Hu TM (2016) Effect of arbuscular mycorrhizal fungi inoculation on cold stress-induced oxidative damage in leaves of *Elymus nutans* Griseb. S Afr J Bot 104:21–9
8. Cobbett CS, Hussain D, Haydon MJ (2003) Structural and functional relationships between type 1B heavy metal-transporting P-type ATPases in Arabidopsis. New Phytol 159: 315–321

9. Colangelo EP, Guerinot ML. Put the metal to the petal: metal uptake and transport throughout plants. Curr Opin Plant Biol. 2006 Jun;9(3):322-30
10. Cui JQ, Hua YP, Zhou T, Liu Y, Huang JY, Yue CP (2020) Global landscapes of the Na^+/H^+ antiporter (NHX) family members uncover their potential roles in regulating the rapeseed resistance to salt stress. Int J Mol Sci 21:3429
11. Dittmer J, Lusseau T, Foissac X, Faoro F (2021) Skipping the insect vector: plant stolon transmission of the phytopathogen '*Ca* Phlomobacter fragariae' from the *Arsenophonus* clade of insect endosymbionts. Insects 12:93
12. Eren E, Arg€uello JM (2004) Arabidopsis HMA2, a divalent heavy metal transporting P1B-type ATPase, is involved in cytoplasmic Zn^{2+} homeostasis. Plant Physiol 136:3712–3723
13. Fu YY, Li FF, Xu T, Cai SJ, Chu WY, Qiu H, Sha S, Cheng GY, Xu QS (2014) Bioaccumulation, subcellular, and molecular localization and damage to physiology and ultrastructure in *Nymphoides peltata* (Gmel.) O. Kuntze exposed to yttrium. Environ Sci Pollut Res 214:2935–42
14. Han YL, Song HX, Liao Q, Yu Y, Jian SF, Lepo JE, Liu Q, Rong XM, Tian C, Zeng J, Guan CY, Ismail AM, Zhang ZH (2016) Nitrogen use efficiency is mediated by vacuolar nitrate sequestration capacity in roots of *Brassica napus*. Plant Physiol 170:1684-1698
15. Hasanuzzaman M, Bhuyan M, Anee TI, Parvin K, Nahar K, Mahmud JA, Fujita M (2019) Regulation of ascorbate-glutathione pathway in mitigating oxidative damage in plants under abiotic stress. Antioxidants 8:384
16. Hermand V, Julio E, Dorlhac de Borne F, Punshon T, Ricachenevsky FK, Bellec A, Gosti F, Berthomieu P (2014) Inactivation of two newly identified tobacco heavy metal ATPases leads to reduced Zn and Cd accumulation in shoots and reduced pollen germination. Metallomics 6:1427-40
17. Higo K, Ugawa Y, Iwamoto M, Korenaga T (1999) Plant *cis*-acting regulatory DNA elements (PLACE) database: 1999. Nucleic Acids Res 27:297-300
18. Hua YP, Feng YN, Zhou T, Xu FS (2017) Genome-scale mRNA transcriptomic insights into the responses of oilseed rape (*Brassica napus* L.) to varying boron availabilities. Plant Soil 416:205-225
19. Hussain D, Haydon MJ, Wang Y, Wong E, Sherson SM, Young J, Camakaris J, Harper JF, Cobbett CS (2004) P-type ATPase heavy metal transporters with roles in essential zinc homeostasis in Arabidopsis. Plant Cell 16:1327-39
20. Hu X, Li T, Xu W, Chai Y (2021) Distribution of cadmium in subcellular fraction and expression difference of its transport genes among three cultivars of pepper. Ecotoxicol Environ Saf 216:112182
21. International Wheat Genome Sequencing Consortium (IWGSC); IWGSC RefSeq principal investigators (2018) Shifting the limits in wheat research and breeding using a fully annotated reference genome. Science 361:eaar7191
22. Jayakodi M, Schreiber M, Stein N, Mascher Martin (2021) Building pan-genome infrastructures for crop plants and their use in association genetics. DNA Res 28: dsaa030

23. Kan M, Yamazaki K, Fujiwara T, Kamiya T (2019) A simple and high-throughput method for xylem sap collection. Biotechniques 67:242-245
24. Kotula L, Garcia Caparros P, Zörb C, Colmer TD, Flowers TJ (2020) Improving crop salt tolerance using transgenic approaches: An update and physiological analysis. Plant Cell Environ 43:2932-2956
25. Lang L, Xu A, Ding J, *et al*. 2017. Quantitative trait locus mapping of salt tolerance and identification of salt-tolerant genes in *Brassica napus* L. Frontiers in Plant Science 8, 1000.
26. Lescot M, Déhais P, ThijsG, Marchal K, MoreauY, Van de PeerY, Rouzé P, Rombauts S. 2002. PlantCARE, a database of plant *cis*-acting regulatory elements and a portal to tools for *in silico* analysis of promoter sequences. Nucleic Acids Research 30, 325-327.
27. Liu HB, Li XH, Xiao JH, Wang SP (2012) A convenient method for simultaneous quantification of multiple phytohormones and metabolites: application in study of rice-bacterium interaction. Plant Methods 8:2
28. Livak KJ, Schmittgen TD (2001) Analysis of relative gene expression data using real-time quantitative PCR and the $2^{-\Delta\Delta C}{}_T$ method. Methods 25:402-408
29. Lv S, Jiang P, Chen X, Fan P, Wang X, Li Y (2012) Multiple compartmentalization of sodium conferred salt tolerance in *Salicornia europaea*. Plant Physiol Biochem 51:47-52
30. Ma S, Wang M, Wu J, Guo W, Chen Y, Li G, Wang Y, Shi W, Xia G, Fu D, Kang Z, Ni F (2021) WheatOmics: A platform combining multiple omics data to accelerate functional genomics studies in wheat. Mol Plant 14:1965-1968
31. Mi H, Muruganujan A, Thomas PD (2013) PANTHER in 2013: modeling the evolution of gene function, and other gene attributes, in the context of phylogenetic trees. Nucleic Acids Res 41:D377-D386
32. Mills RF, Peaston KA, Runions J, Williams LE (2012) HvHMA2, a P1BATPase from barley, is highly conserved among cereals and functions in Zn and Cd transport. PLoS One 7: e42640
33. Nakano Y, Asada K (1981) Hydrogen peroxide is scavenged by ascorbate-specific peroxidase in spinach chloroplasts. Plant Cell Physiol 22:867–80
34. Nguyen N, Wang D (2020) Multiview learning for understanding functional multiomics. PLoS Comput Biol 16:e1007677
35. Nocito FF, Lancilli C, Dendena B, Lucchini G, Sacchi GA (2011) Cadmium retention in rice roots is influenced by cadmium availability, chelation and translocation. Plant Cell Environ 34:994-1008
36. Ogawa I, Nakanishi H, Mori S, Nishizawa NK (2009) Time course analysis of gene regulation under cadmium stress in rice. Plant Soil 325:97–108
37. Park J, Song WY, Ko D, Eom Y, Hansen TH, Schiller M, Lee TG, Martinoia E, Lee Y (2012) The phytochelatin transporters AtABCC1 and AtABCC2 mediate tolerance to cadmium and mercury. Plant J 69:278–288
38. Qin X, Xia Y, Hu C, Yu M, Shabala S, Wu S, Tan Q, Xu S, Sun X (2021) Ionomics analysis provides new insights into the co-enrichment of cadmium and zinc in wheat grains. Ecotoxicol Environ Saf

223:112623

39. Raza A, Habib M, Kakavand SN, Zahid Z, Zahra N, Sharif R, Hasanuzzaman M (2020) Phytoremediation of cadmium: physiological, biochemical, and molecular mechanisms. Biology 9:177
40. Rimbert H, Darrier B, Navarro J, Kitt J, Choulet F, Leveugle M, Duarte J, Rivière N, Eversole K; International Wheat Genome Sequencing Consortium, Le Gouis J; on behalf The BreedWheat Consortium, Davassi A, Balfourier F, Le Paslier MC, Berard A, Brunel D, Feuillet C, Poncet C, Sourdille P, Paux E. High throughput SNP discovery and genotyping in hexaploid wheat. PLoS One 13:e0186329
41. Rizwan M, Ali S, Abbas T, Zia-Ur-Rehman M, Hannan F, Keller C, Al-Wabel MI, Ok YS (2016) Cadmium minimization in wheat: A critical review. Ecotoxicol Environ Saf 130:43-53
42. Sasaki A, Yamaji N, Ma JF (2014) Overexpression of OsHMA3 enhances Cd tolerance and expression of Zn transporter genes in rice. J Exp Bot 65:6013–6021
43. Sasaki A, Yamaji N, Yokosho K, Ma JF (2012) Nramp5 is a major transporter responsible for manganese and cadmium uptake in rice. Plant Cell 24:2155–2167.
44. Satoh-Nagasawa N, Mori M, Nakazawa N, Kawamoto T, Nagato Y, Sakurai K, Takahashi H, Watanabe A, Akagi H (2012) Mutations in rice (*Oryza sativa*) heavy metal ATPase 2 (OsHMA2) restrict the translocation of zinc and cadmium. Plant Cell Physiol 53:213–224
45. Smith TF, Waterman MS (1987) Identification of common molecular subsequences. J Mol Biol 147:195–197
46. Sui FQ, Chang JD, Tang Z, Liu WJ, Huang XY, Zhao FJ (2018) Nramp5 expression and functionality likely explain higher cadmium uptake in rice than in wheat and maize. Plant Soil 433:377–389
47. Sun WJ, Zhang JC, Ji XL, Feng ZQ, Wang X, Huang WJ, You CX, Wang XF, Hao YJ (2021) Low nitrate alleviates iron deficiency through regulating iron homeostasis in apple. Plant Cell Environ 44:1869-1884
48. Takahashi R, Ishimaru Y, Shimo H, Ogo Y, Senoura T, Nishizawa NK, Nakanishi H (2012) The OsHMA2 transporter is involved in root-to-shoot translocation of Zn and Cd in rice. Plant Cell Environ 35:1948-57
49. Tan J, Wang J, Chai T, Zhang Y, Feng S, Li Y, Zhao H, Liu H, Chai X (2013) Functional analyses of TaHMA2, a P1B-type ATPase in wheat. Plant Biotechnol J 11:420–431
50. Wong CKE, Jarvis RS, Sherson SM, Cobbett CS (2009) Functional analysis of the heavy metal binding domains of the Zn/Cd-transporting ATPase, HMA2, in *Arabidopsis thaliana*. New Phytol 181:79-88
51. Wu H, Shabala L, Azzarello E, et al (2018) Na^+ extrusion from the cytosol and tissue-specific Na^+ sequestration in roots confer differential salt stress tolerance between durum and bread wheat. J Exp Bot 69:3987-4001
52. Xu C, Li Z, Wang J (2022) Temporal and tissue-specific transcriptome analyses reveal mechanistic insights into the *Solidago canadensis* response to cadmium contamination. Chemosphere 4:133501

53. Yu JJ, Jin X, Sun XM, Gao TX, Chen XM, She YM, Jiang TB, Chen SX, Dai SJ (2017) Hydrogen peroxide response in leaves of poplar (*Populus simonii* × *Populus nigra*) revealed from physiological and proteomic analyses. Int J Mol Sci 18:2085
54. Zhang L, Gao C, Chen C, Zhang W, Huang XY, Zhao FJ (2020) Overexpression of rice OsHMA3 in wheat greatly decreases cadmium accumulation in wheat grains. Environ Sci Technol 54:10100-10108
55. Zhang M, Zhang J, Lu L, Zhu Z, Yang X (2016) Functional analysis of CAX2-like transporters isolated from two ecotypes of *Sedum alfredii*. Biol Plant 60:37–47
56. Zhang Q, Chen H, He M, Zhao Z, Cai H, Ding G, Shi L, Xu F (2017) The boron transporter BnaC4.BOR1;1c is critical for inflorescence development and fertility under boron limitation in *Brassica napus*. Plant Cell Environ 40:1819-1833
57. Zhang ZH, Zhou T, Liao Q, Yao JY, Liang GH, Song HX, Guan CY, Hua YP (2018) Integrated physiologic, genomic and transcriptomic strategies involving the adaptation of allotetraploid rapeseed to nitrogen limitation. BMC Plant Bio 18:322
58. Zhang ZH, Zhou T, Tang TJ, Song HX, Guan CY, Huang JY, Hua YP (2019) A multiomics approach reveals the pivotal role of subcellular reallocation in determining rapeseed resistance to cadmium toxicity. J Exp Bot 70:5437-5455
59. Zhao KF, Fan H, Zhou S, Song J (2003) Study on the salt and drought tolerance of *Suaeda salsa* and *Kalanchoe claigremontiana* under iso-osmotic salt and water stress. Plant Sci 165:837-844
60. Zhou T, Hua Y, Huang YP, Ding GD, Shi L, Xu FS (2016) Physiological and transcriptional analyses reveal differential phytohormone responses to boron deficiency in *Brassica napus* genotypes. Front Plant Sci 7:221
61. Zhou T, Yue CP, Liu Y, Zhang TY, Huang JY, Hua YP (2021) Multiomics reveal pivotal roles of sodium translocation and compartmentation in regulating salinity resistance in allotetraploid rapeseed. J Exp Bot 72:5687-5708

Figures

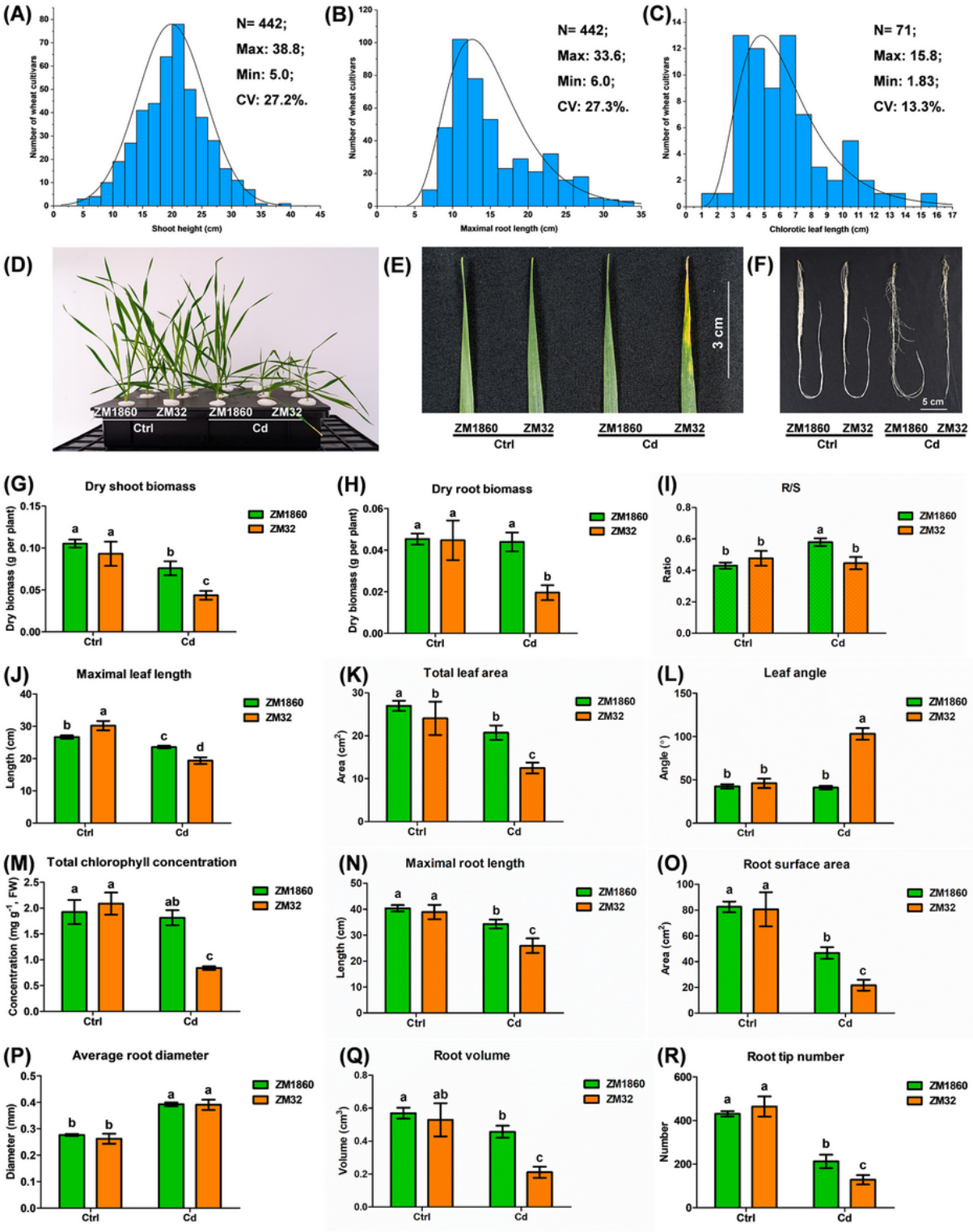

Figure 1

Natural variations in wheat cadmium (Cd) resistance and morpho-physiological identification of the resistant and sensitive wheat genotypes. **(A-B)** Natural variations of Cd resistance in a panel comprising 442 accessions, as represented by maximal leaf **(A)** and root length **(B)**. **(C)** Variations of Cd sensitivity in a panel comprising 71 Cd-sensitive genotypes, as represented by chlorotic leaf length **(C)**. **(D)** Growth performance of 'Zhengmai 1860' ('ZM1860') and 'Zhoumai 32' ('ZM32') under Cd-free (control) and 10

μM Cd ($CdCl_2$) conditions. **(E-F)** Images of mature leaves **(E)** and roots **(F)**. **(G-R)** Dry shoot biomasses **(G)**, dry root biomasses **(H)**, root/shoot ratios **(I)**, maximal leaf lengths **(J)**, total leaf areas **(K)**, leaf angles **(L)**, leaf chlorophyll concentrations **(M)**, maximal root length **(N)**, root surface areas **(O)**, average root diameters **(P)**, root volumes **(Q)**, and root tip numbers **(R)** of 'ZM1860' and 'ZM32' under control and 10 μM Cd conditions. All wheat plants were grown hydroponically under 10 μM Cd for 14 d. The data are presented as the mean ± s.d., and the different letters indicate statistically significant differences ($P < 0.05$, one-way analysis of variance (ANOVA) with post-hoc Tukey's test).

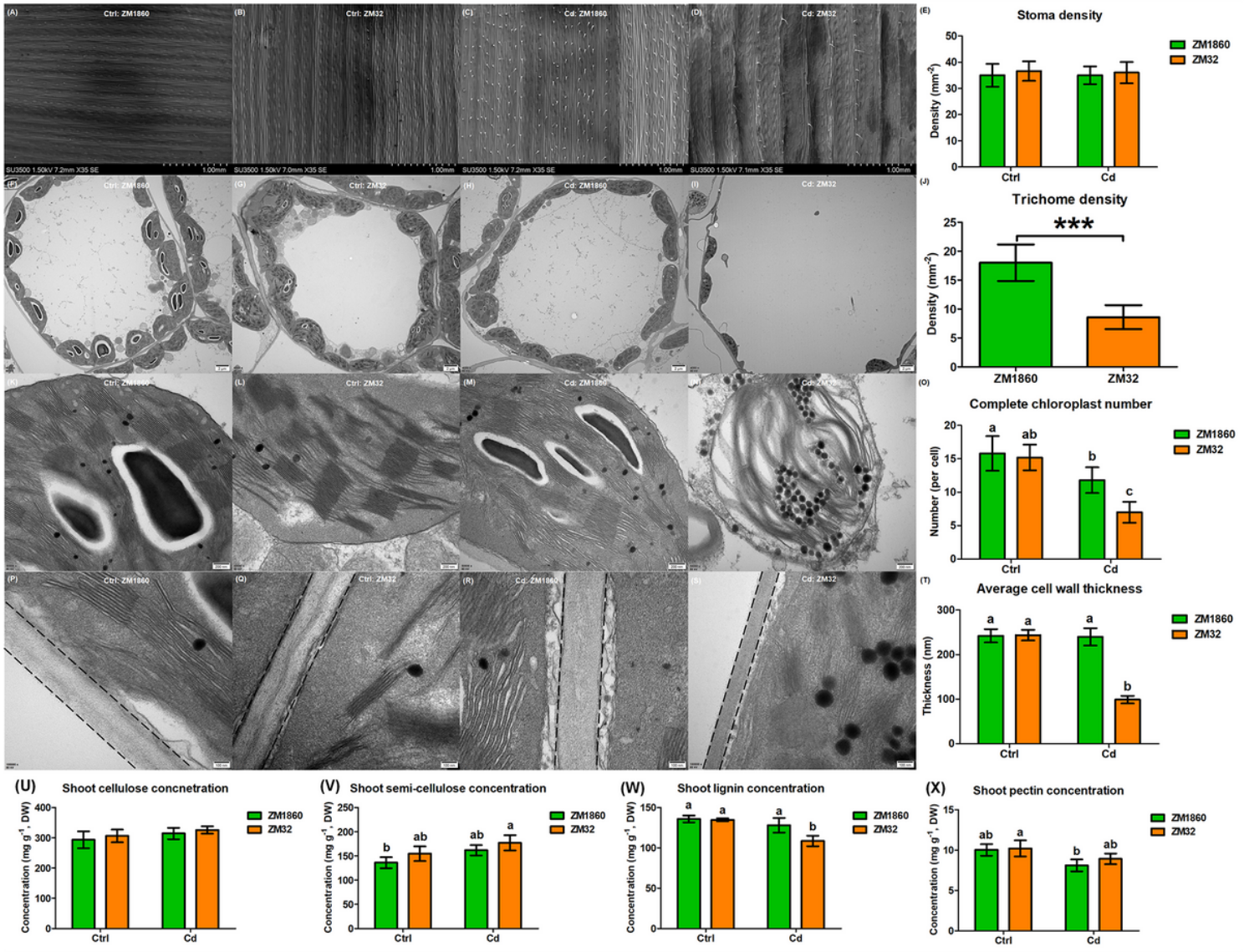

Figure 2

Leaf ultrastructure of the Cd-resistant wheat genotype 'ZM1860' and the Cd-sensitive wheat genotype 'ZM32'. **(A–D)** Scanning electron microscopy images of the leaves under **(A, B)** Cd-free (control) and **(C, D)** 10 μM Cd conditions. **(E, J)** Comparative analysis of stoma **(E)** and trichome **(J)** density between 'ZM1860' and 'ZM32'. **(F–I, K-N)** Low-magnification **(F-I)** and close-up **(K-N)** view of chloroplasts arrayed along plasma membranes and cell morphologies under Cd-free (control) and 10 μM Cd conditions. **(O)** Comparative analysis of complete chloroplast number between 'ZM1860' and 'ZM32'. **(P-S)** Transmission

electron microscopy images of cell wall morphology under **(P, Q)** Cd-free (control) and **(R, S)** 10 μM Cd conditions. **(T)** Comparative analysis of cell wall thickness between 'ZM1860' and 'ZM32'. All the wheat plants were grown hydroponically under 10 μM Cd for 14 d until sampling. For **Fig. 2E, J, O, and T**, data are means (±s.d.), n=5. Different letters indicate significant differences as determined by ANOVA and Tukey's HSD test ($P < 0.05$).

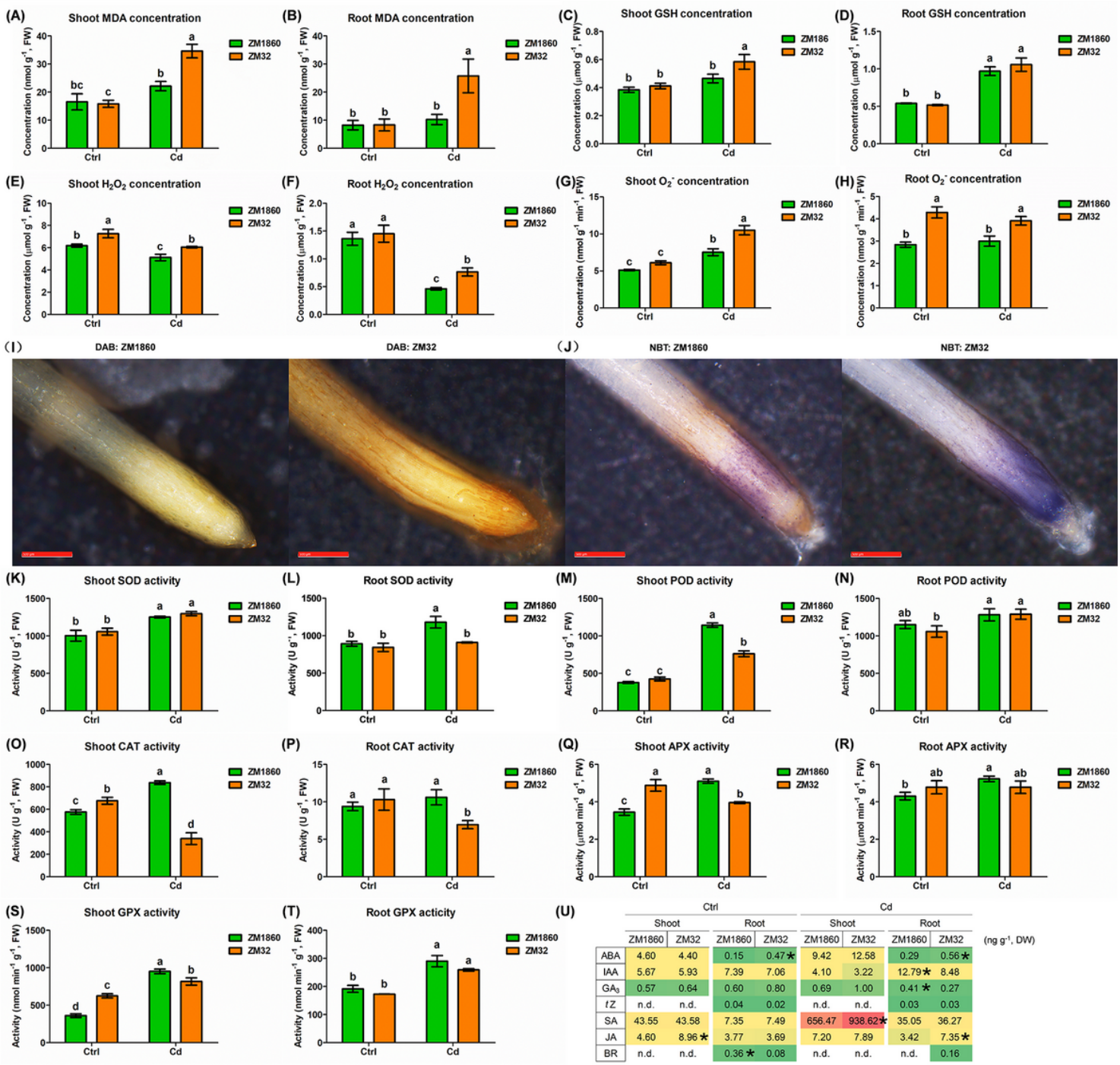

(U)

	Ctrl				Cd				
	Shoot		Root		Shoot		Root		(ng g^{-1}, DW)
	ZM1860	ZM32	ZM1860	ZM32	ZM1860	ZM32	ZM1860	ZM32	
ABA	4.60	4.40	0.15	0.47★	9.42	12.58	0.29	0.56★	
IAA	5.67	5.93	7.39	7.06	4.10	3.22	12.79★	8.48	
GA_3	0.57	0.64	0.60	0.80	0.69	1.00	0.41★	0.27	
tZ	n.d.	n.d.	0.04	0.02	n.d.	n.d.	0.03	0.03	
SA	43.55	43.58	7.35	7.49	656.47	938.62★	35.05	36.27	
JA	4.60	8.96★	3.77	3.69	7.20	7.89	3.42	7.35★	
BR	n.d.	n.d.	0.36★	0.08	n.d.	n.d.	n.d.	0.16	

Figure 3

Comparative analysis of reactive oxygen species homeostasis and phytohormone profiling in the Cd-resistant and Cd-sensitive genotypes. **(A-H)** Concentrations of MDA **(A, B)**, GSH **(C, D)**, H_2O_2 **(E, F)**, and O_2^- **(G, H)** in the shoots **(A, C, E, G)** and roots **(B, D, F, H)** under control and Cd conditions. **(I, J)** DAB **(I)** and NBT **(J)** staining of the roots under Cd toxicity. **(K-T)** Activity of SOD **(K, L)**, POD **(M, N)**, CAT **(O, P)**, APX **(Q, R)**, and GPX **(S, T)** in the shoots **(K, M, O, Q, S)** and roots **(L, N, P, R, T)** under control and Cd conditions. **(U)** Phytohormone concentrations in the shoots and roots under control and Cd conditions. All the wheat plants were grown hydroponically under 10 μM Cd for 14 d until sampling. Data are means (±s.d.), n=3. Different letters indicate significant differences as determined by ANOVA and Tukey's HSD test ($P < 0.05$).

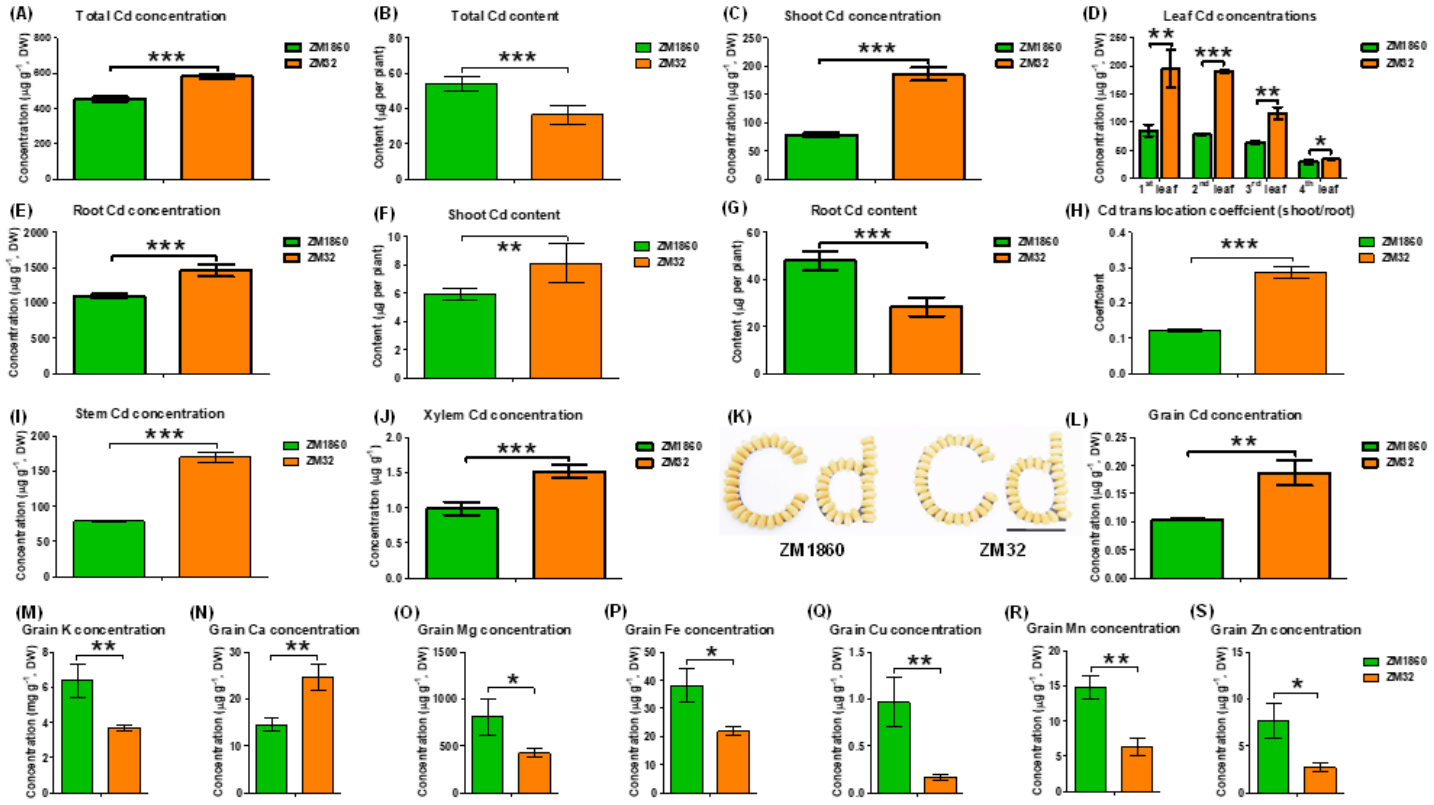

Figure 4

Comparative analysis of Cd concentrations between the Cd-resistant genotype and Cd-sensitive genotypes. **(A)** Total plant Cd concentrations, **(B)** total plant Cd content, **(C)** whole shoot **(C)** Cd concentrations, **(D)** Cd concentrations in different leaves, **(E)** root Cd contention, **(F-G)** whole shoot **(F)** and root **(G)** Cd content, **(H)** coefficients of Cd translocation from roots to shoots, **(I, J)** stem **(I)** and xylem **(J)** Cd concentrations, **(K)** wheat grains, **(L-R)** concentrations of Cd **(K)**, K **(L)**, Ca **(M)**, Mg **(N)**, Fe **(O)**, Cu **(P)**, Mn **(Q)**, and Zn **(R)** in wheat grains harvested at the maturity stage of wheat plants. For Fig. 2A-J, all the wheat plants were grown hydroponically under 10 μM Cd for 14 d; for Fig. 2K-R, the wheat plants were grown hydroponically under 10 μM Cd for the whole growth stage until harvesting. Data are means (± s.d.), n=5. Significant differences were determined using Student's *t*-test: *, $P < 0.05$; **, $P < 0.01$; ***, $P < 0.001$.

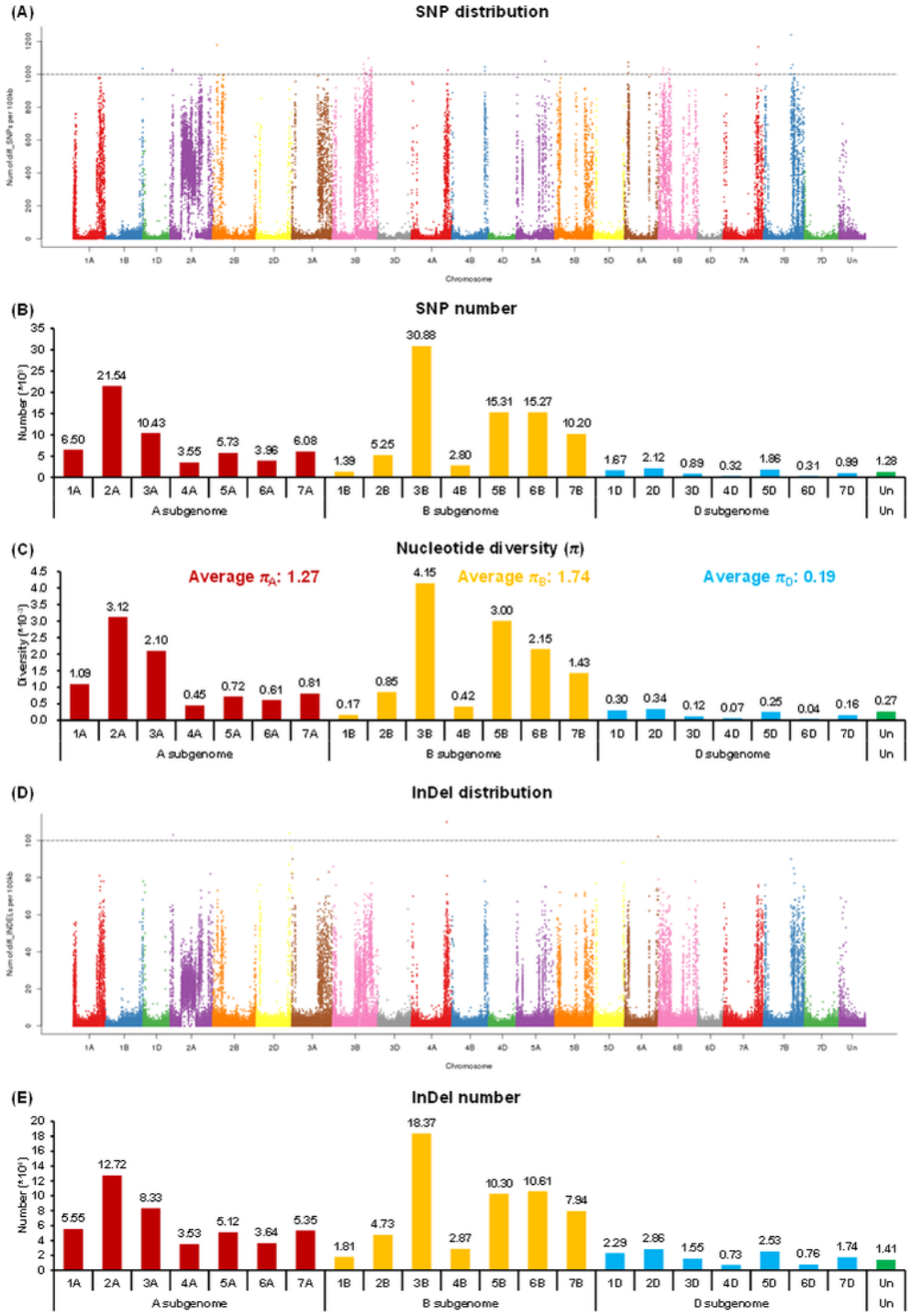

Figure 5

Distribution and number of genome-wide single nucleotide polymorphisms (SNPs) and insertions/deletions (InDels) between the Cd-resistant and Cd-sensitive genotypes. (A, B) Chromosomal distribution (A) and number (B) of SNPs. (C) Nucleotide diversity (π) on each chromosome. (D, E) Chromosomal distribution (D) and number (E) of InDels. For **Fig. 5A and D**, the x-axis represents the

wheat chromosome sizes (Mb) while the y-axis represents the number of SNPs or InDels present at that point on each chromosome.

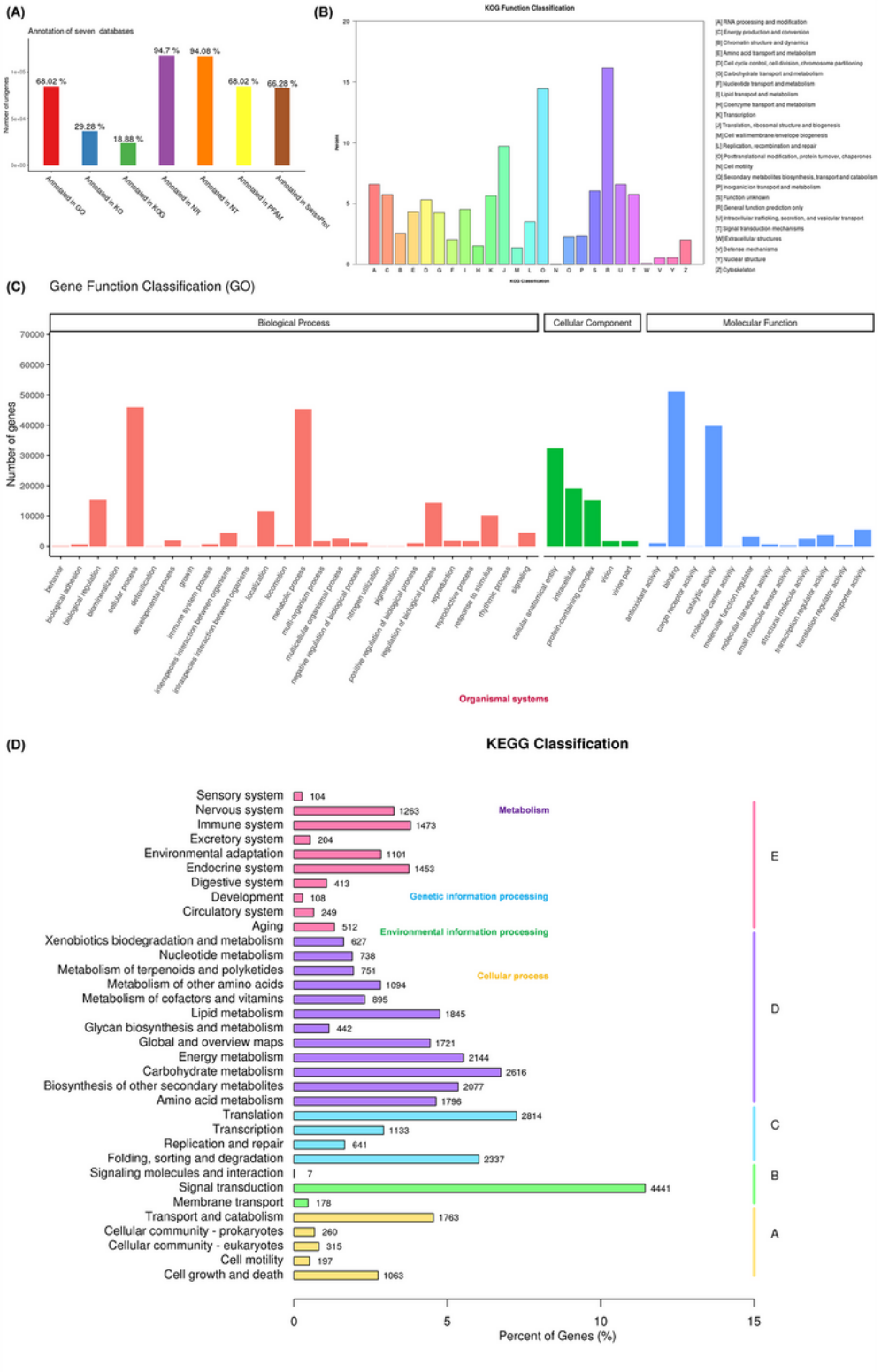

Figure 6

Overview of whole-genome re-sequencing data for the Cd-resistant and Cd-sensitive genotypes. **(A)** Percentage of the polymorphic unigenes annotated in databases. **(B-D)** Enrichment analysis of KOG term

(B), GO classification **(C),** and KEGG pathway **(D)** involving the genome-wide DNA variants.

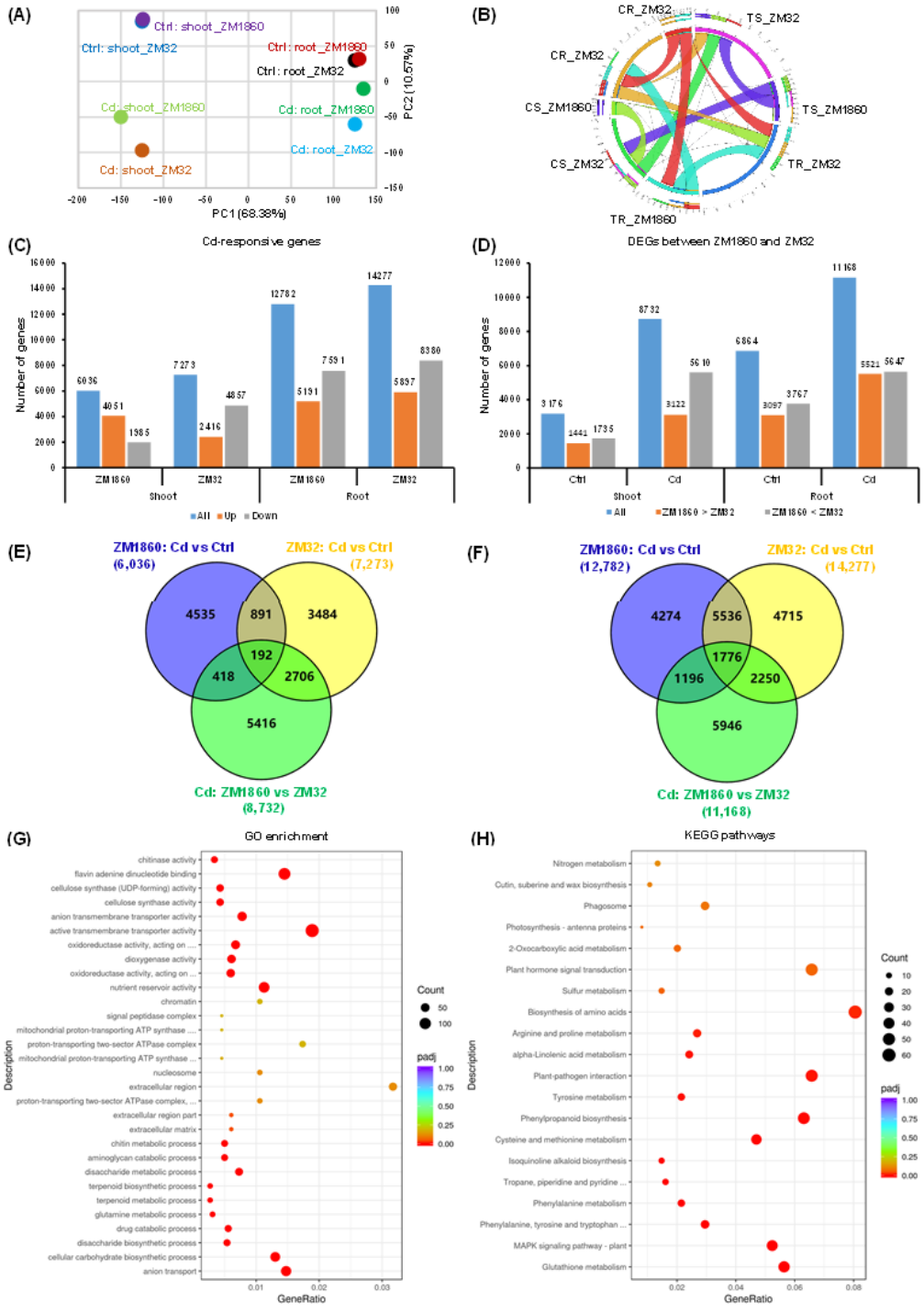

Figure 7

Overview of transcriptome sequencing data for the Cd-resistant and Cd-sensitive genotypes. **(A)** Principal component analysis of the RNA-seq samples. **(B)** Circos diagram (http://circos.ca/) showing *Pearson* correlations between the RNA-seq samples. The thickness of the lines indicates the correlation between

each pair of RNA-seq samples: the thicker the lines, the higher the correlation. **(C, D)** Number of the genome-wide Cd-responsive differential expressed genes (DEGs) in the shoots and roots between the Cd-resistant and Cd-sensitive genotypes. Up, upregulation; down, downregulation. **(E, F)** Venn diagrams for DEGs in the shoots **(E)** and roots **(F)**. **(G, H)** GO term and KEGG pathway enrichment analysis of the global DEGs. The circle size indicates the number of DEGs, and the rich factor indicates the degree of enrichment of the GO terms and KEGG pathways involving DEGs.

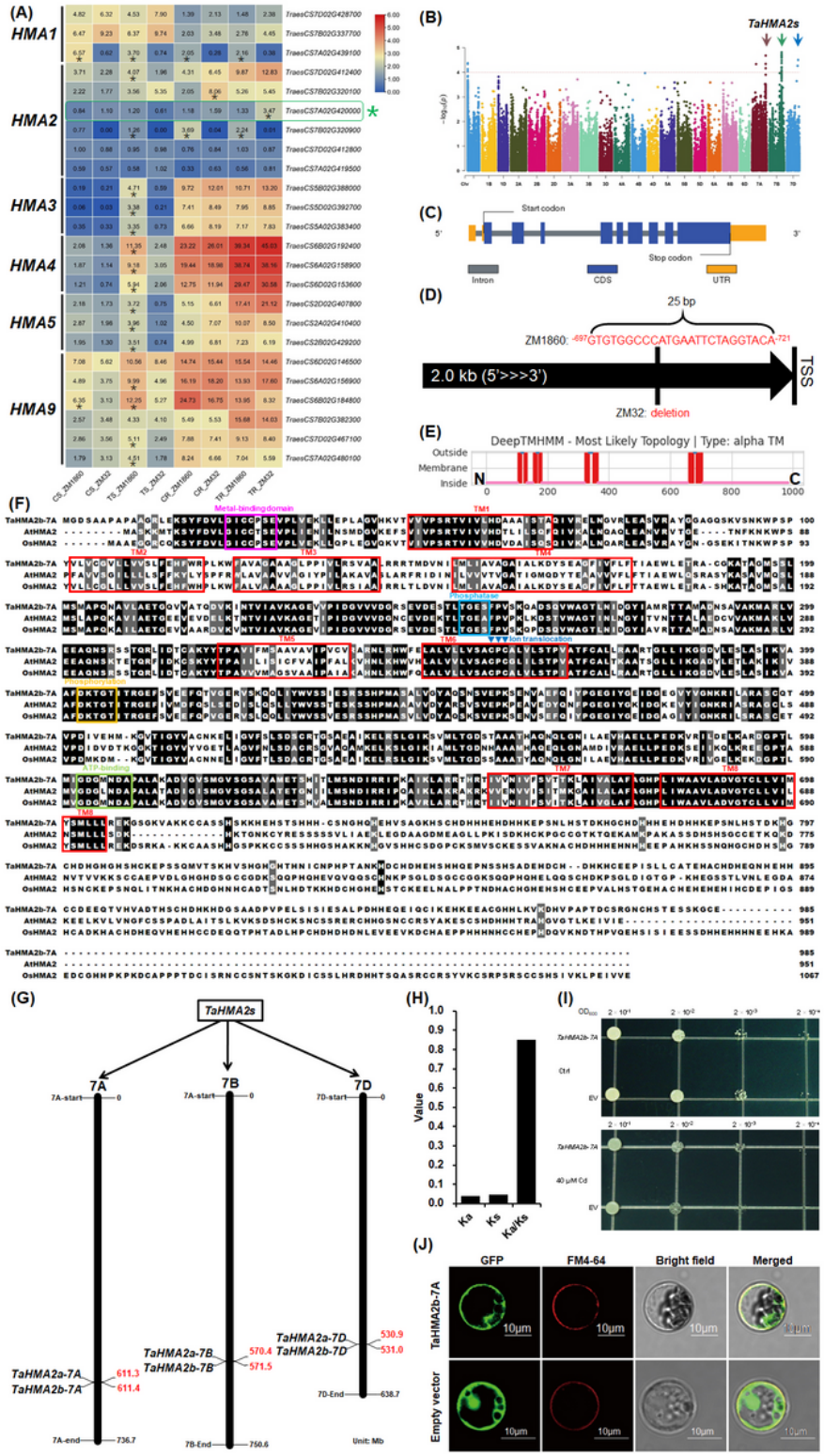

Figure 8

Identification and characterization of the core HMA family members responsible for the differences in Cd resistance between the Cd-resistant and Cd-sensitive genotypes. **(A)** Transcriptional profiling of genome-wide HMAs in the shoots and roots under control and Cd toxicity conditions. The heatmap shows gene expression levels as indicated by the FPKM values. The differentially expressed genes (DEGs) with higher expression between the Cd-resistant and Cd-sensitive genotypes are denoted by asterisks. **(B)** Genome-wide association analysis of maximal root length under 10 μM $CdCl_2$ in a wheat population consisting 206 genotypes, which were genotyped by **Zhou et al. (2021)**. **(D)** Gene structure **(C)** and sequence differences **(D)** in the promoter regions of *TaHMA2b-7A* in the Cd-resistant (ZM1860) and Cd-sensitive (ZM32) genotypes. CDS, coding sequence; TSS, transcription starting site; UTR, untranslated region. **(E)** Predicted topology of TaHMA2b-7A in the membrane. The numbers indicate the location of amino acids along the polypeptide of TaHMA2b-7A. **(F)** Multiple alignment of the amino acid sequences of AtHMA2, OsHMA2, and TaHMA2b-7A. Identical residues are in black and similar residues are shaded. TGES, part of the phosphatase domain; DKTGT, site of aspartyl phosphate formation; GDGxNDA, ATP-binding motif; CPC, ion translocation. **(G)** Physical mapping of six *HMA2* homologs in allohexaploid wheat. **(H)** Selection pressure analysis of TaHMA2b-7A in Cd-resistant and Cd-sensitive genotypes based on the non-synonymous (Ka) and synonymous (Ks) substitution rates. **(I)** Cd resistance assay of *TaHMA2b-7A* transformed yeast (INVSc1) cells. EV, empty vector (*pYES2*). **(J)** GFP-assisted subcellular localization analysis of TaHMA2b-7A.

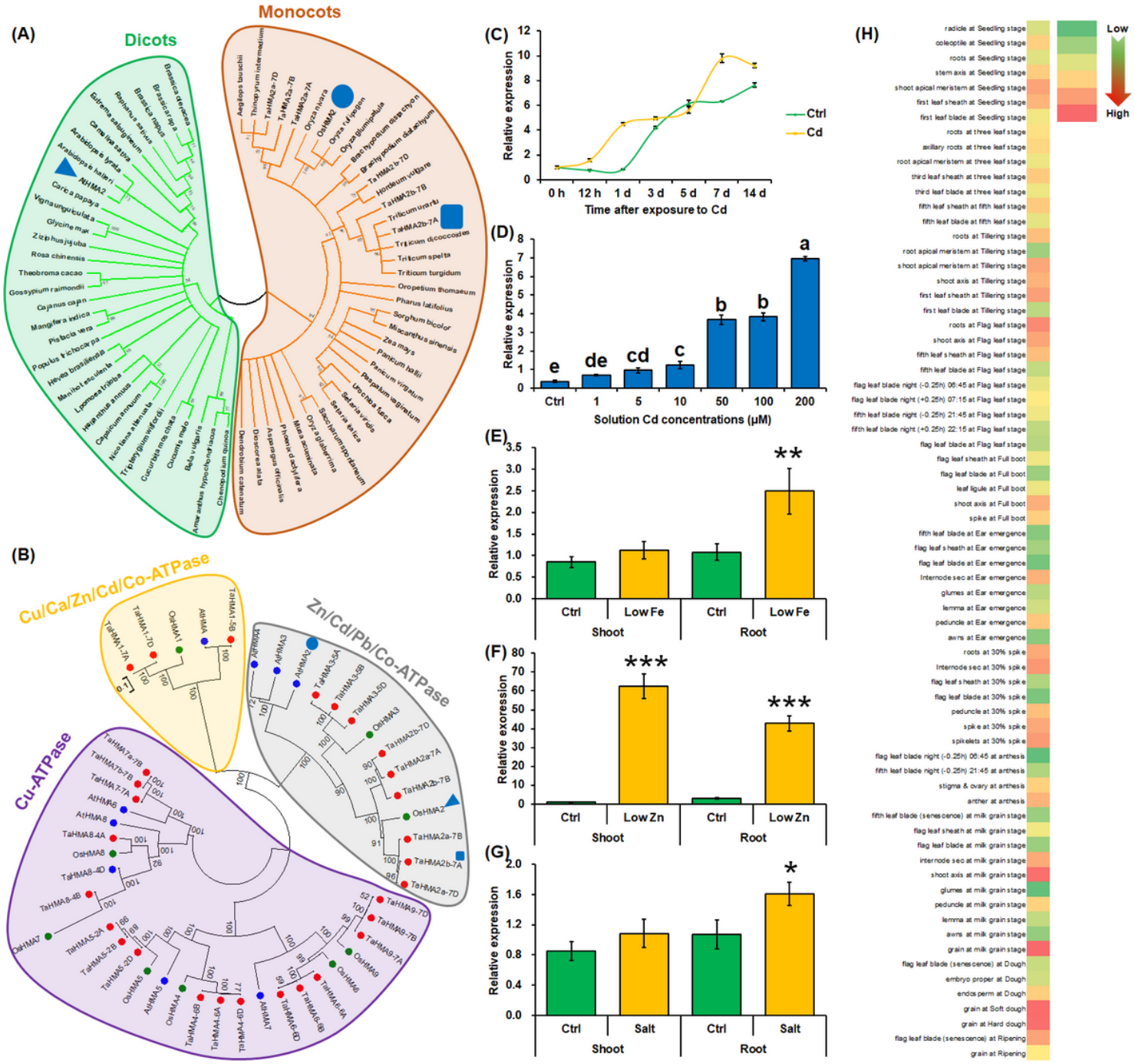

Figure 9

Phylogenetic analysis and spatio-temporal expression profiling of *TaHMA2b-7A*. **(A)** Phylogenetic relationships of HMA2s in dicots and monocots; **(B)** phylogenetic relationships of HMAs in Arabidopsis (*Arabidopsis thaliana* L.), rice (*Oryza sativa* L.), and wheat (*Triticum aestivum* L.). The evolutionary history was inferred using the neighbor-joining method in MEGA v.6.06 (http://www.megasoftware.net/). The scale bar indicates 0.01 substitutions per site. Bootstrap values are indicated adjacent to the corresponding node. **(C)** Relative expression of *TaHMA2b-7A* at different time-points after exposure to 10 μM Cd. Uniform wheat plants were grown hydroponically under Cd-free condition for 5 d, and then the plants were transferred to 10 μM Cd. **(D-H)** Relative expression of *TaHMA2b-7A* under different solution

Cd concentrations **(D)**; relative expression of *TaHMA2b-7A* under low iron (Fe) condition **(E)**; relative expression of *TaHMA2b-7A* under low zinc (Zn) condition **(F)**; relative expression of TaHMA2b-7A under salt stress **(G)**; relative expression of *TaHMA2b-7A* in different tissues at the whole growth stage **(H)**.

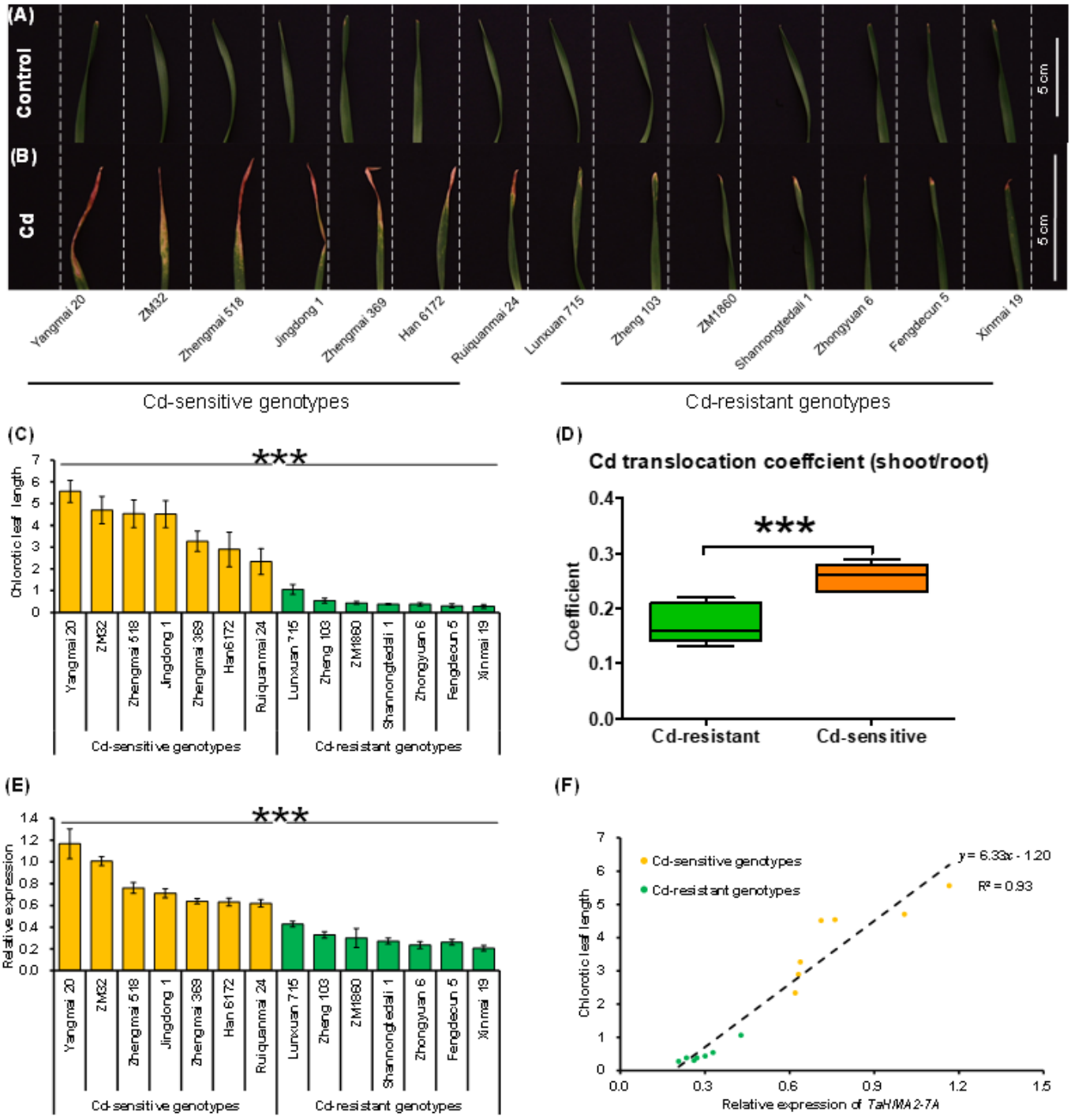

Figure 10

Association analysis of *TaHMA2b-7A* expression and wheat Cd resistance. **(A, B)** Leaf performance of the Cd-resistant and Cd-sensitive genotypes under control **(A)** and Cd toxicity **(B)** conditions. Uniform wheat plants after seed germination were grown hydroponically under control and 10 μM Cd for 14 d. **(C)** Chlorotic leaf length of the Cd-resistant and Cd-sensitive genotypes under Cd toxicity for 14 d. **(D)** Translocation coefficients of Cd from roots to shoots in the Cd-resistant and Cd-sensitive genotypes. **(E)** Relative expression of *TaHMA2b-7A* in the roots of the Cd-resistant and Cd-sensitive genotypes under Cd toxicity. **(F)** Correlation of chlorotic leaf length and root *TaHMA2b-7A* expression of the Cd-resistant and Cd-sensitive genotypes under Cd toxicity. For **Fig. 10C, D, and E**, data are means (± s.d.), n=3. Significant differences were determined using Student's *t*-test: *, $P < 0.05$; **, $P < 0.01$; ***, $P < 0.001$.

Supplementary Files

This is a list of supplementary files associated with this preprint. Click to download.

- Supplementaryfigures.docx
- Supplementarytables.docx